

AFGL-TR-88-0325

Model Studies of the Polar Ionosphere: Final Report

Robert E. Sheehan

Boston College
140 Commonwealth Avenue
Chestnut Hill, MA 02167

21 November 1988

Final Report
28 August 1985 - 27 November 1988

Approved for public release; distribution unlimited

DTIC
ELECTE
APR 18 1989
S E D
cb

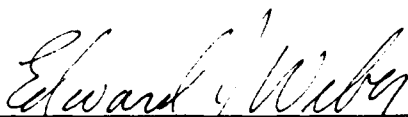
AIR FORCE GEOPHYSICS LABORATORY
AIR FORCE SYSTEMS COMMAND
UNITED STATES AIR FORCE
HANSCOM AIR FORCE BASE, MASSACHUSETTS 01731-5000

89 4 18 039

AD-A206 821

4

"This technical report has been reviewed and is approved for publication"

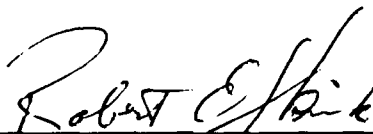


EDWARD J. WEBER
Contract Manager



WILLIAM K. VICKERY
Acting Branch Chief

FOR THE COMMANDER



ROBERT A. SKRIVANEK
Division Director

This report has been reviewed by the ESD Public Affairs Office (PA) and is releasable to the National Technical Information Service (NTIS).

Qualified requestors may obtain additional copies from Defense Technical Information Center. All others should apply to the National Technical Information Service.

If your address has changed, or if you wish to be removed from the mailing list, or if the addressee is no longer employed by your organization, please notify AFGL/DAA, Hanscom AFB, MA 01731. This will assist us in maintaining current mailing list.

Do not return copies of this report unless contractual obligations or notice on a specific document requires that it be returned.

UNCLASSIFIED

SECURITY CLASSIFICATION OF THIS PAGE

REPORT DOCUMENTATION PAGE

Form Approved
OMB No. 0704-0188

1a. REPORT SECURITY CLASSIFICATION Unclassified			1b. RESTRICTIVE MARKINGS			
2a. SECURITY CLASSIFICATION AUTHORITY			3. DISTRIBUTION/AVAILABILITY OF REPORT Approved for public release; distribution unlimited			
2b. DECLASSIFICATION/DOWNGRADING SCHEDULE						
4. PERFORMING ORGANIZATION REPORT NUMBER(S)			5. MONITORING ORGANIZATION REPORT NUMBER(S) AFGL-TR-88-0325			
6a. NAME OF PERFORMING ORGANIZATION Trustees of Boston College		6b. OFFICE SYMBOL (If applicable)	7a. NAME OF MONITORING ORGANIZATION Air Force Geophysics Laboratory			
6c. ADDRESS (City, State, and ZIP Code) 140 Commonwealth Avenue Chestnut Hill, MA 02167			7b. ADDRESS (City, State, and ZIP Code) Hanscom Air Force Base, MA 01731-5000			
8a. NAME OF FUNDING / SPONSORING ORGANIZATION		8b. OFFICE SYMBOL (If applicable)	9. PROCUREMENT INSTRUMENT IDENTIFICATION NUMBER F19628-85-K-0051			
8c. ADDRESS (City, State, and ZIP Code)			10. SOURCE OF FUNDING NUMBERS			
			PROGRAM ELEMENT NO. 62101F	PROJECT NO. 4643	TASK NO. 08	WORK UNIT ACCESSION NO. AI
11. TITLE (Include Security Classification) Model Studies of the Polar Ionosphere: Final Report						
12. PERSONAL AUTHOR(S) Robert E. Sheehan						
13a. TYPE OF REPORT Final		13b. TIME COVERED FROM 8-28-85 TO 11-27-88		14. DATE OF REPORT (Year, Month, Day) 1988 November 21		
15. PAGE COUNT 88						
16. SUPPLEMENTARY NOTATION						
17. COSATI CODES			18. SUBJECT TERMS (Continue on reverse if necessary and identify by block number)			
FIELD	GROUP	SUB-GROUP	Ionospheric model			
19. ABSTRACT (Continue on reverse if necessary and identify by block number) This report presents modifications and additions to an ionospheric chemistry program that models the high latitude-polar cap ionosphere (1-dimensional along a magnetic field line; 100-600 km altitude). Interest principally centers on effects of soft (1 kev) electron fluxes typically observed precipitating into the polar cap ionosphere. Major changes involved incorporating an existing (0+ diffusion code with the Strickland local (E _f region) ionospheric chemistry code and the addition of electron and ion temperature calculations based the diffusion code. Also included are calculations of Hall and Pedersen electric conductivities and a separate program that determines electric currents in the ionosphere based on the model result; these were used in conjunction with measurements from the PIIE rocket campaign in February, 1985. Some details of the numerical methods employed in the various calculations are given, as well as an overview of the programming logic -- (continued on back page						
20. DISTRIBUTION/AVAILABILITY OF ABSTRACT <input type="checkbox"/> UNCLASSIFIED/UNLIMITED <input type="checkbox"/> SAME AS RPT. <input type="checkbox"/> DTIC USERS			21. ABSTRACT SECURITY CLASSIFICATION Unclassified			
22a. NAME OF RESPONSIBLE INDIVIDUAL Edward J. Weber			22b. TELEPHONE (Include Area Code)		22c. OFFICE SYMBOL AFGL/LIS	

19. ABSTRACT (continued)

and a step-by-step description of program execution. The Strickland flux transport program that calculates production rates input to the chemistry model remains essentially unchanged but, a new parameterization scheme ~~has been de-~~veloped that could have applications to global problems requiring a large number of flux calculations.

Table of Contents

Figure Captions	iv
1. Introduction	1
2. Details of the Model	4
A. Overview	4
B. Chemistry	6
C. Diffusion	11
D. Ionospheric Temperature	20
3. Running the Ionospheric Chemistry Model	25
4. Parameterization of the Flux Transport Model	31
A. Motivation	31
B. Outline of the Strickland Flux Transport Model	32
C. Constructing the Tables	34
D. Results and Examples	36
5. PIIE Results	38
References	43
Tables	45
Figures	52



Accession For	
NTIS GRA&I	<input checked="" type="checkbox"/>
DTIC TAB	<input type="checkbox"/>
Unannounced	<input type="checkbox"/>
Justification	
By	
Distribution/	
Availability Codes	
Dist	Avail and/or Special
A-1	

Figure Captions

Figure 1. Flow chart showing the major elements of the ionospheric chemistry model.

Figure 2. Electron density profiles from 0-60 minutes using precipitating electron flux from the PIIE rocket experiment; local chemistry only (no O⁺ diffusion).

Figure 3. Same as Figure 2 but including O⁺ diffusion.

Figure 4a-d. Same as Figure 2 (0-10 minutes) but with high altitude boundary O⁺ flux set at $1 \times 10^{12} \text{ m}^{-2} \text{ s}^{-1}$ (down), 1×10^{10} (down), 1×10^{10} (up), and 5×10^{12} (up), respectively.

Figure 5. Schematic showing the contribution to production by flux= ϕ_1 at energy= E_5 .

Figure 6a-f. Altitude profiles of production rates for O₂⁺, O⁺, and N₂⁺ contributed by $\phi_1 = 1 \times 10^5 \text{ (cm}^{-2} \text{ s}^{-1} \text{ sr}^{-1} \text{ eV}^{-1}\text{)}$ at E=55, 180, 320, 550, 750, and 1300 eV.

Figure 7. Differential electron flux measured by the AFGL PIIE rocket experiment within an auroral arc on March 15, 1985.

Figure 8a. Maxwellian flux with 200 eV characteristic energy.

Figure 8b. Production rate profiles calculated from the tables for the flux in Figure 8a.

Figure 9. PIIE observations of electron density fluctuations, total electron density, electron temperature, and energy flux of precipitating electrons vs. time (seconds after launch), altitude, and UT. Vertical line indicates time of the model calculation inside the arc.

Figure 10. Model production rates of O⁺(4S), N⁺ and N₂⁺. Also shown is the plasma heating rate normalized to the ambient electron density. The curves labelled (a) and (b) refer to the electron density profiles, shown in Figure 12, that are used in the flux transport code. Production rates corresponding to each curve are nearly identical.

Figure 11. Ten point averages of PIIE electron differential flux measurements (downgoing electrons). Sample from 282.3 to 288.1 s is used to model inside the arc. Other sample is used to establish an initial electron density profile for the ionospheric chemistry model.

Figure 12. Electron density and T_e results from the chemistry model using the rates shown in Figure 10. Densities shown correspond to rates calculated for curve (a).

Figure 13. Hall and Pedersen electric conductivities for the 5 minute profile in Figure 12.

Figure 14. Calculated PIIE electron density profiles corresponding to flux durations of 1-30 minutes. Initial O+ density is 10^4 cm^{-3} at all altitudes.

Figure 15. Same as Figure 14 except starting from a lower initial electron density (10^3 cm^{-3}).

Figure 16. Decay of electron density profile after flux is turned off.

Figure 17. Development of electron density profile using electron flux outside arc.

Figure 18. Same as Figure 17 except starting from a lower initial electron density (10^3 cm^{-3}).

Figure 19. Calculated electron density profiles using flux inside arc and a cold neutral atmosphere ($T_n=750 \text{ K}$).

Figure 20. Same as Figure 19 except with a hotter neutral atmosphere ($T_n=1200\text{K}$).

1. Introduction

A realistic model of the ionosphere is an extremely complicated physical and mathematical problem. Excitation and ionization by precipitating particles or solar radiation influence chemical reactions at every altitude. Diffusion along field lines and horizontal transport determine the final electron and ion densities at any point. These local, unsteady processes are superimposed on global and secular variations having diurnal, seasonal, and solar-cycle dependences.

In the auroral zone and polar cap it is clear that precipitating electrons and protons have a profound effect on the ionospheric plasma density. However, electric fields may convect F-region plasma hundreds or thousands of kilometers from its source; hence, optical emissions and density fluctuations associated with large scale plasma structures can also occur some distance away from direct sources of ionization. Although satellites, rockets, radars, and photometers have probed ionospheric structures in detail, the origin and fate of plasma in the polar cap remain difficult problems. A reliable model of ionospheric response to ionizing sources would help to unravel some difficulties by defining the portion of ionization produced locally.

Many researchers have modeled the ionosphere with varying degrees of complexity depending primarily on the application (Jones and Rees, 1973; Roble and Rees, 1977; Schunk et al., 1986). Global descriptions under different geophysical conditions rely heavily on large scale empirical studies; physical models based on the governing equations have been limited by the availability of key parameters and computational difficulties. The ability to test and refine a model has grown with the aid of coordinated experiments, comprehensive data sets, and large, high-speed computers.

The model developed by D. Strickland and colleagues has two distinct parts, flux transport and ionospheric chemistry. Flux transport begins with a specified differential electron flux at some upper altitude boundary and calculates electron fluxes throughout the ionospheric depth. This is accomplished by a fast and accurate solution of the flux transport equation that treats both elastic and inelastic scattering by the principal neutral species, N_2 , O_2 , and O . A table of cross sections for inelastic scattering and neutral densities describe the details of each interaction. An eigenvalue representation solves for differential fluxes over a range of altitudes and energies at 20 pitch angles from 0 to 180 degrees. Production rates for selected ionic and neutral species are found from the calculated fluxes and tabulated cross sections for ionization and various excitations. The original code with electron fluxes has been extended by Strickland to include both precipitating protons and solar EUV input; results in this report come from earlier versions with electron fluxes only.

Production rates from the transport part, whatever the source of ionization, become inputs to the ionospheric chemistry model. Our attention has centered on modifying the chemistry programs to handle production generated by soft (1 keV) fluxes of electrons typically observed over polar cap auroral arcs. This interest required some changes inherent in F-region physics, chiefly by the integration of an existing O^+ diffusion code (written by Rob Danniell) with local chemistry and the addition of new electron and ion temperature calculations. The following sections describe these codes with some applications and discuss remaining problems and goals.

The major scientific application of this study can be found in Weber et al. (1988), which analyzes results from the PIIE rocket experiment conducted in Greenland on March 15, 1985. To complement dc electric field measurements

taken during the flight. Hall and Pedersen electric conductivity calculations were added to the model based on standard expressions involving calculated electron densities and temperatures. Combining this information with the measured electric fields, a separate program determined field-aligned currents from the continuity equation and tensor conductivity.

In a separate effort in support of the AFGL airborne ionospheric observatory, J. Fleischman participated in several missions and became involved in improving the collection system of navigational data needed for mission analysis. A Zenith Z-248 laptop computer was programmed for storage of INS data to back up the existing tape system and for a running presentation of current navigational data and related navigational problems. A manual describing the system and its operation was written by J. Fleischman as a technical report.

The bulk of this report centers on mathematical details and physical assumptions in the model code because the model is essentially a tool which should be applied thoughtfully in light of its limitations. In any case, a knowledgeable user will eventually become familiar with these details and will adjust the internal workings of the model and the peripheral procedures to suit his own purposes and tastes.

2. Details of the Model

A. Overview

Designed for E-region applications, the original code solved local chemical rate equations for the species listed in Table 1. Later, O⁺ diffusion was added to extend the altitude range into the F-region. We made structural changes in the programs to allow the chemical rate and diffusion coefficients to reflect density information from each part. In addition, instead of assuming a fixed electron temperature (T_e) profile, we developed a code to solve the electron heat conduction equation based on the computed electron density. The electron plasma heating rate is supplied by the same flux transport code that calculates chemical production rates.

The flow chart in Figure 1 illustrates the procedure followed by the model as it now stands. The lower half pertains to ionospheric chemistry and thermal energy balance. Inputs are production rate ($\text{cm}^{-3} \text{ s}^{-1}$). Starting with initial density profiles for all the species and an initial T_e profile, the code integrates the quantities (densities and T_e) until some desired time interval has elapsed or equilibrium is reached. Since diffusion and heat conduction are represented by partial differential equations in time and altitude, appropriate boundary conditions are also required.

Because T_e responds very quickly to changes in the heating rate, time steps must be very short at first to handle potentially large temperature variations. During the first second after $t=0$, a cycle through the basic program unit (THERM, CHEM, and O⁺ DIFFUS) is performed every .1 second. From $t=1$ to 120 s the update, dt , is lengthened to 1 s; after 120 s, $dt=10$ s. These times are appropriate for the types of conditions we have encountered, but since the internal logic of each unit is the same, regardless the time increment dt , experimentation is not difficult. In fact, each program unit has its own internal time step (calculated in CHEM and O⁺ DIFFUS, set in THERM), so

that the overall update time dt only affects the overhead incurred in recomputing various coefficients.

At the start of an arbitrary time interval, t_n , THERM calculates the thermal conduction coefficient for electrons from the current values of electron density, n_e , and T_e . It then solves for T_e at a time $t_{n+1} = t_n + \delta t$ using coefficients which are assumed constant during δt . The new T_e resets temperature dependent chemical rate coefficients for density calculations in CHEM. When all densities except O+ are found at time t_{n+1} , the new chemical rate (from CHEM) and T_e dependent diffusion coefficient for O+ go to O+ DIFFUS, which finds the O+ density at t_{n+1} . The resulting total electron density ($n_e = n_i$) and T_e at $t = t_{n+1}$ now become inputs to THERM for the next cycle beginning at t_{n+1} . By requiring that the overall update time, dt , reflects the fastest changing quantity, in this case T_e , we can minimize errors introduced by solutions with constant coefficients over discrete time intervals. A more elaborate treatment would entail representative, average values of the coefficients and an update time calculated to ensure a specified accuracy.

At present both the electron flux transport and chemistry codes are one dimensional with dependences only along a magnetic field line. Given the complexity of the existing transport code, this most likely will remain a practical limitation; however, if the electron gyroradius is small compared with the horizontal extent of the incident flux, true for most auroral arcs, the approximation is acceptable. Chemical lifetimes, on the other hand, are comparable to transport times of F-region density structures by convection electric fields. When this occurs integration times must be held small or convection velocities must be assumed to lie along a constant density structure like an arc.

Temporal variations pose a somewhat different problem. Although flux transport is a steady state formulation, the time required to establish production rates are short (1s) and effectively vary with the input flux. A separate flux transport calculation

would be required for each new incident flux, not a practical undertaking in most cases. However, if spectral shapes are similar, scaling the production rates relative to an absolute flux could mimic temporal flux variations. Production rates passed to the chemistry code are held constant, or, after operating for a designated time, can be switched off to simulate decay of ion density. There is no reason why direct production by an incident flux must be fixed in CHEM; the only requirement is that variations be slow compared with the time steps in the integrating routines.

Each basic code unit, CHEM, O+ DIFFUS, and THERM involves the continuity equation for scalar quantity, ion density (internal energy), of the form

$$\frac{\partial f}{\partial t} = \nabla \cdot \underline{S} + q - l \quad (2.1)$$

where f is ion (energy) density in ion (eV) cm^{-3} , S is a flux in ions (eV) in $\text{cm}^{-2} \text{s}^{-1}$, and q and l are source and loss terms, respectively, in ions (eV) $\text{cm}^{-3} \text{s}^{-1}$. In one dimension the only spatial variation is altitude, or more accurately along a magnetic field line where $dh=ds \sin I$, h =altitude, s =distance along B (magnetic field), and I =inclination of B . Near the poles B is nearly vertical and $dh \geq ds$ which we assume here.

B. Chemistry

Since diffusion is relatively unimportant in the lower ionosphere, densities of various species are governed by a system of local chemical rate equations,

$$\frac{\partial N_i}{\partial t} = P_i + \sum_{m,n} k_{mn} N_m N_n - N_i \sum_m l_m N_m - \alpha_i N_i \sum_m N_m \quad (2.2)$$

P_i represents direct production by any process, e.g., electron impact; k_{mn} are rate coefficients for reactions involving species m and n that produce species i . Similarly, l_m and α_i describe loss reactions with species m and recombination with electrons ($n_e = \sum n_i$), respectively. The rate coefficients k , l , and α are read from an input data file when the program starts. We have modified some rates and added reactions to the set supplied with the original Strickland code based on a table in VallanceJones (1974). The rates can be changed directly in the input file or through the Cyber UPDATE utility. Rates depending on the electron temperature are interpolated from a table computed with the current T_e profile.

Subroutine CHEMEQ performs the integration of (2.2) for each species over a time step beginning at T and ending at $T+DTUP$. Starting with densities calculated from the previous step, a preparatory routine, DERIV, computes the necessary coefficients and calculates densities for those species designated as "fast", which adjust quickly to changes in production and loss and hence are close to equilibrium at all times. Assuming $\partial N_i / \partial t_i = 0$ for the fast species, $N_i = p_i / q_i$. The species list (Table 1) is arranged so that all the "slow" species to be integrated appear first starting with index 5, after which the "fast" species are listed. Unless otherwise noted, species 5 through 10 (NO^+ , O_2^+ , O^+ , $N(4S)$, and $N(2D)$) are numerically integrated in the examples shown in this report. Species 11 through 20 are assumed to be in equilibrium in the sense described above.

The numerical integration routine CHEMEQ employs a second order predictor-corrector scheme. Letting Y represent the density, N , we can express (2.2) as

$$\frac{dY}{dt} = C - D \quad (2.3)$$

where C is production and $D = Y/\tau$ stands for the loss term which is proportional the independent variable, Y . Using an internal time step t , chosen to reflect the fastest changing species, a finite difference representation of (2.3) involves quantities at the initial time, t_0 , and final time, t_0+t ,

$$\frac{Y - Y_0}{2 \left(\frac{t}{2} \right)} = C_0 - \frac{\left(\frac{Y + Y_0}{2} \right)}{t_0} \quad (2.4)$$

The denominator in the LHS of (2.4) emphasizes that the finite difference is a second order representation of the time derivative at the midpoint; accordingly, the RHS is an average ($C = C_0$, and $\tau = \tau_0$).

From (2.4) a predicted value of Y after a time interval t can be found,

$$Y_p = \frac{[Y_0 (2 \tau_0 - t) + 2 \tau_0 t C_0]}{(2 \tau_0 + t)} \quad (2.5)$$

With the predicted value of Y_p new average values of τ and C can be calculated to yield a corrected value Y after another application of (2.5).

$$\bar{\tau} = \frac{1}{2} \left(\frac{Y_0}{D_0} + \frac{Y_p}{D_p} \right) = \frac{1}{2} (\tau_0 + t)$$

$$C = \frac{1}{2} (C_0 - C_p)$$

$$Y_C = \frac{[Y_0 (2\tau - t) + 2\tau + C]}{(2\tau + t)}$$

(2.6)

Predicted values for C and τ at $t = t_0 + t$ are evaluated by a call to subroutine DERIV. If Y_C fails a convergence criterion the time step t is reduced and the procedure repeated.

Up to order t^2 , the integration method in CHEMEQ is identical to results obtained from a standard modified Euler numerical integration. Using the same terminology as above, the predicted Euler value is simply a linear extrapolation from the initial value,

$$Y_p = Y_0 + Y_0' t = Y_0 + \left(C_0 - \frac{Y_0}{t_0} \right) t$$

(2.7)

A corrected slope is obtained from an average with the predicted value,

$$Y'_{ave} = \frac{1}{2} (Y_0' + Y_p')$$

$$= \frac{1}{2} \left[\left(C_0 - \frac{Y_0}{\tau_0} \right) + \frac{Y_0 + \left(C_0 - \frac{Y_0}{\tau_0} \right) t}{\tau_0} \right]$$

(2.8)

The corrected value then becomes,

$$\begin{aligned}
Y_{C \text{ Euler}} &= Y_0 + Y'_{\text{ave}} t \\
&= \frac{Y_0 \left(2\tau_0 - 2t + \frac{t^2}{\tau_0} \right)}{2\tau_0} + C_0 t \frac{(2\tau_0 - t)}{2\tau_0}
\end{aligned}
\tag{2.9}$$

Expanding the denominator in (2.5) by a Taylor series we get,

$$\begin{aligned}
\frac{1}{2\tau_0 + t} &= \frac{\left(1 + \frac{t}{2\tau_0} \right)^{-1}}{2\tau_0} \\
&= \frac{1}{2\tau_0} \left(1 - \frac{t}{2\tau_0} + \frac{t^2}{(2\tau_0)^2} + \dots \right)
\end{aligned}
\tag{2.10}$$

so that,

$$Y_p = Y_0 (2\tau_0 - t) \frac{\left(1 - \frac{t}{2\tau_0} + \frac{t^2}{(2\tau_0)^2} \right)}{2\tau_0} + C_0 2\tau_0 t \frac{\left(1 - \frac{t}{2\tau_0} + \frac{t^2}{(2\tau_0)^2} \right)}{2\tau_0}
\tag{2.11}$$

or,

$$Y_p = \frac{Y_0 \left(2\tau_0 - 2t + \frac{t^2}{\tau_0} \right)}{2\tau_0} - \frac{Y_0 \frac{t^3}{4\tau_0^3}}{2\tau_0} + \frac{C_0 t (2\tau_0 - t)}{2\tau_0} + \frac{C_0 \frac{t^3}{2\tau_0}}{2\tau_0}$$

$$= Y_c \text{Euler} + O(t^3)$$

$$(2.12)$$

C. Diffusion

General discussions about vertical transport in the ionosphere can be found in Rishbeth and Garriot (1969) and Banks and Kockarts (1973). The starting point is an expression for the diffusion velocity W_d of an ion along a magnetic field line,

$$W_d = -D_a \sin^2 I \left(\frac{1}{N} \frac{dN}{dz} + \frac{1}{T_p} \frac{dT_p}{dz} + \frac{1}{H_p} \right)$$

$$(2.13)$$

D_a is the plasma diffusion coefficient, N the ion density, z the distance along a field line, $T_p = (T_i + T_e)/2$ the plasma temperature, and $H_p = 2kT_p/m_i \nu_{in}$ where ν_{in} is the ion-neutral collision frequency. For vertical field lines $\sin^2 I = 1$, and with the flux $S = NW_d$, (2.1) becomes

$$\frac{\partial N}{\partial t} = \frac{\partial}{\partial z} \left(-ND_a \left(\frac{1}{N} \frac{\partial N}{\partial z} + \frac{1}{T_p} \frac{\partial T_p}{\partial z} + \frac{1}{H_p} \right) \right) + (q-l)$$

$$(2.14)$$

Expanding (2.14) we get

$$\begin{aligned}
\frac{\partial N}{\partial t} = & \left[Da \right] \frac{\partial^2 N}{\partial z^2} + Da \left[\frac{1}{Da} \frac{\partial Da}{\partial z} + \frac{1}{T_p} \frac{\partial T_p}{\partial z} + \frac{1}{H_p} \right] \frac{\partial N}{\partial z} \\
& + Da \left[\frac{1}{Da T_p} \frac{\partial T_p}{\partial z} \frac{\partial Da}{\partial z} - \frac{1}{T_p^2} \left(\frac{\partial T_p}{\partial z} \right)^2 + \frac{1}{T_p} \frac{\partial^2 T_p}{\partial z^2} \right. \\
& \left. + \frac{1}{Da H_p} \frac{\partial Da}{\partial z} - \frac{1}{H_p^2} \frac{\partial H_p}{\partial z} \right] N + [q-1]
\end{aligned}
\tag{2.15}$$

This is a second order, parabolic, partial differential equation in $N(z,t)$ of the form,

$$\frac{\partial N(z,t)}{\partial t} = A(z) \frac{\partial^2 N}{\partial z^2} + B(z) \frac{\partial N}{\partial z} + C(z) N + D(z)
\tag{2.16}$$

The coefficients A, B, C, and D are altitude dependent parameters which can be identified with the quantities in brackets in (2.15).

Analytic solutions are possible only under special conditions, e.g., diffusive equilibrium ($dN/dt=0$) and simple dependencies for the coefficients. Numerical solutions permit more realistic coefficients and even allow time dependent coefficients as long as the integration time step is sufficiently short for them to be considered constant. This became crucial after we added a calculation for T_e which affects the plasma temperature T_p .

A diffusion equation requires both an initial condition, in this case an altitude profile of O^+ density at time $t=0$, and boundary conditions. The low altitude boundary

is chosen low enough so that the O+ density calculated from local chemistry (CHEM) can supply one condition. At the upper boundary it is more realistic to set the slope of the O+ density which is related to the flux of ions across the boundary. This flux can either be set manually or estimated from scale height arguments. Lacking measurements or reliable estimates of the flux, one can test for a range of values into and out of the ionosphere. There is a critical value of outgoing flux that drives densities negative in the solution, thereby setting an upper limit of upward flux. A similar situation also occurs in the T_e calculation.

The diffusion equation is solved numerically by a Crank-Nicolson scheme (Gerald and Wheatley, 1984) starting with a finite difference representation of (2.16).

$$\begin{aligned}
 \frac{\partial u_i^{j+1/2}}{\partial t} &= \frac{u_i^{j+1} - u_i^j}{T} = \\
 \frac{A_i}{2} &\left[\frac{u_{i+1}^j - 2u_i^j + u_{i-1}^j}{H^2} + \frac{u_{i+1}^{j+1} - 2u_i^{j+1} + u_{i-1}^{j+1}}{H^2} \right] \\
 &+ \frac{B_i}{2} \left[\frac{u_{i+1}^j - u_{i-1}^j}{2H} + \frac{u_{i+1}^{j+1} - u_{i-1}^{j+1}}{2H} \right] \\
 &+ \frac{C_i}{2} [u_i^j + u_i^{j+1}] + \frac{D_i^j + D_i^{j+1}}{2}
 \end{aligned}
 \tag{2.17}$$

where $u(t,z)=u$ is density. Index j corresponds to time incremented by T and i corresponds to altitude incremented by H . Both the time and spatial derivatives are represented by central difference approximations with errors of order Δx .

$$\left(\frac{df}{dx}\right)_i = \frac{f_{i+1} - f_{i-1}}{2\Delta x} + O(\Delta x)^2$$

$$\left(\frac{d^2f}{dx^2}\right)_i = \frac{f_{i+1} - 2f_i + f_{i-1}}{2\Delta x} + O(\Delta x)^2$$

Since $\partial u / \partial t$ is evaluated at the midpoint of the time interval $(j,j+1)$, spatial derivatives at the midpoint are approximated by averages evaluated at the beginning and end of the time interval.

Equation (2.16) expresses unknown densities at time $j+1$ in terms of known densities at t . Collecting terms, we get

$$\begin{aligned} & u_{i-1}^{j+1} \left(-\frac{A_i}{2H^2} + \frac{B_i}{4H} \right) + u^{j+1} \left(\frac{A_i}{H^2} - \frac{C_i}{2} + \frac{B_i}{T} \right) + u_{-1}^{j+1} \left(-\frac{A_i}{2H^2} - \frac{B_i}{4H} \right) \\ & = u_{-1}^j \left(\frac{A_i}{2H^2} - \frac{B_i}{4H} \right) + u^j \left(-\frac{A_i}{H^2} + \frac{C_i}{2} + \frac{B_i}{T} \right) + u_{+1}^j \left(\frac{A_i}{2H^2} + \frac{B_i}{4H} \right) \end{aligned}$$

(2.18)

The coefficients in (2.18) are determined in O+ DIFFUS and recast in the following equation,

$$\begin{aligned} & u_{i-1}^{j+1} DM_i + u^{j+1} EM_i + u_{+1}^{j+1} FM_i \\ & = u_{-1}^j DB_i + u^j EB_i + u_{+1}^{j+1} FB_i + D_i = BM_i \end{aligned}$$

(2.19)

Within the main loop of the CHEM program the coefficients A, B, C, D, and hence DM, EM, etc. are constant in time. The right side of (2.19) contains densities at the end of the prior time step j (initial altitude profile at j=0, t=0). Since (2.19) couples densities at 3 adjacent altitudes at the end of the next time step, j+1, in terms of quantities from the previous time step, a full altitude profile at time t_{j+1} requires solving a set of linear equations for u_i^{j+1} , $i=0$ to n, corresponding to z_0 (low altitude boundary) to z_n (high altitude boundary). This tridiagonal system is solved by an efficient Gauss elimination method with the sole restriction that the altitude spacing H be less than $A_i/2B_i$ for all i. An implicit scheme involving several altitudes at t_{j+1} , as in (2.19), has the virtue of stability for all values of the coefficients as opposed to explicit methods which handle each altitude independently.

Equation (2.19) applies as shown except at the boundaries, z_0 and z_n . Since the O_2 density at the lower boundary is held at the current local chemistry value, $u_0^{j+1} = u_0^j$. Thus (2.19) becomes

$$\begin{aligned} u_0^{j+1}DM_1 + u_1^{j+1}EM_1 + u_2^{j+1}FM_1 \\ = u_0^j DB_1 + u_1^j EB_1 + u_2^j FB_1 \end{aligned}$$

or, because $DM = -DB$,

$$\begin{aligned} u_0^{j+1}DM_1 + u_1^{j+1}EM_1 + u_2^{j+1}FM_1 \\ = u_0^j DB_1 + u_1^j EB_1 + u_2^j FB_1 \end{aligned}$$

(2.20)

To incorporate the upper boundary flux condition into the solution, we begin with (2.13) ($N \Rightarrow u$). The flux of O^+ crossing the upper boundary (positive upward) is given by

$$\begin{aligned}\phi_n = u_n W_d &= -u_n D_a \sin^2 i \left(\frac{1}{u_n} \frac{du_n}{dz} + \frac{1}{T_p} \frac{dT_p}{dz} + \frac{1}{H_p} \right) \\ &= - \left(F \frac{du_n}{dz} + G u_n \right) = -Q_n\end{aligned}$$

(2.21)

A positive value for the parameter Q_N indicates a downward net flux through the upper altitude boundary. From (2.21), the slope of the O^+ density at the upper boundary can be specified by a central difference approximation that gives a value for u_{n+1} required by (2.17).

$$\begin{aligned}\frac{du_n}{dz} &= \frac{Q_n - G u_n}{F} = \frac{u_{n+1} - u_{n-1}}{2H} \\ u_{n+1} &= u_{n-1} + 2H \frac{Q_n - G u_n}{F}\end{aligned}$$

Again collecting terms as in (2.18),

$$\begin{aligned}
& u_{n-1}^{j+1} \left(-\frac{A_n}{H^2} \right) + u_n^{j+1} \left[\left(\frac{A_n}{H^2} - \frac{C_n}{2} \right) + \frac{G}{F} \left(\frac{A_n}{H} + \frac{B_n}{2} \right) + \frac{1}{T} \right] \\
& = u_{n-1}^j \left(\frac{A_n}{H^2} \right) + u_n^j \left[\frac{1}{T} - \left(\frac{A_n}{H^2} - \frac{C_n}{2} \right) - \frac{G}{F} \left(\frac{A_n}{H} + \frac{B_n}{2} \right) \right] + CQ_n + D_n \\
& \quad CQ_n = \frac{2}{F} \left(\frac{A_n}{H} + \frac{B_n}{2} \right) Q_n
\end{aligned}
\tag{2.22}$$

At the upper boundary (2.19) becomes

$$\begin{aligned}
& u_{n-1}^{j+1} DM_n + u_n^{j+1} EM_n + \\
& = u_{n-1}^j DB_n + u_n^j EB_n + CQ_n + D_n = BM_n
\end{aligned}
\tag{2.23}$$

The system of equations represented by (2.19), (2.20) and (2.21) can be summarized by a $n \times n$ matrix equation,

$$\begin{array}{ccccccc}
EM_1 & FM_1 & 0 & \dots & \dots & \dots & \dots \\
DM_2 & EM_2 & FM_2 & 0 & \dots & \dots & \dots \\
0 & \dots & \dots & \dots & \dots & \dots & 0 \\
\dots & 0 & DM_i & EM_i & FM_i & 0 & \dots \\
0 & \dots & \dots & \dots & \dots & \dots & 0 \\
\dots & \dots & \dots & 0 & DM_{n-1} & EM_{n-1} & FM_{n-1} \\
\dots & \dots & \dots & \dots & 0 & DM_n & EM_n
\end{array}$$

$$\tag{2.24}$$

The internal time step $dt=T$ is estimated from a truncated version of (2.14),

$$\frac{\partial n}{\partial t} = - \frac{\partial}{\partial z} \left(D_a \frac{\partial N}{\partial z} \right)$$

(2.25)

To evaluate (2.25) an explicit expression for D_a and N are needed.

$$D_a = \frac{H_p v}{g}$$

where H_p is the ion (O^+) plasma scale height,

$$H_p = \frac{k(T_e + T_i)}{m_i g}$$

and v is the ion-neutral collision frequency. The e and i indices for the temperatures and mass refer to electron and ion; k is the Boltzmann coefficient and g is the gravitational acceleration. $N(z)$ can be approximated in terms of the scale height by

$$N(z, t) = N_0(t) e^{-\frac{z-z_0}{H_p}}$$

leading to,

$$\frac{\partial N}{\partial z} = - \frac{N}{H_p}$$

Substituting these into (2.25) we get

$$\frac{\Delta N}{\Delta t} = D_a \frac{N}{H_p^2} - \frac{dD_a}{dz} \frac{N}{H_p}$$

$$= D_a \frac{N}{H_p^2} \left(1 - \frac{H_p}{D_a} \frac{dD_a}{dz} \right)$$

or

$$\Delta t = \frac{\Delta N}{N} \frac{H_p g}{n} \left(1 - \frac{H_p}{D_a} \frac{dD_a}{dz} \right)^{-1} \quad (2.26)$$

If we require the relative density change to be small, $\Delta N/N = \epsilon (= .01, \text{ e.g.})$, and set $H_p g/v = \tau$, (2.26) becomes

$$\Delta t = \frac{\epsilon \tau}{\left(1 - \frac{H_p}{D_a} \frac{dD_a}{dz} \right)} = \frac{\epsilon \tau}{\left(1 - \frac{H_p}{H_d} \right)} \quad (2.27)$$

The second term in the denominator of (2.27), the ratio of the plasma scale height to the diffusion scale height, influences the final δt . At high altitudes (600 km, e.g.) H_p is typically 5-10 times larger than H_d . At lower altitudes H_p/v decreases and $H_p \approx H_d$, which means that Δt increases rapidly. Thus, usually only the highest altitude is required to determine the shortest Δt necessary for the diffusion calculation.

The following examples (Figures 2 and 3) illustrate some diffusion results. They all are derived from the same incident electron flux measured on the PIIE rocket flight (Weber et al., 1987). The upper and lower boundaries are at 600 km and 120 km, respectively; the altitude spacing is 10 km. In these examples both the electron and ion temperature profiles do not change ($T_e = 1000\text{K}$, $T_e = 2000\text{K}$, $T_e = 1500\text{K}$, at 600 km). The effect of diffusion can be seen most readily by comparing Figure 2 (local chemistry only) with Figure 3 (local chemistry and O^+ diffusion). Both figures begin

with the same initial electron (=total ion) density profile at $t=0$, and show successive electron density profiles at 10 min intervals up to 1 hr. With local chemistry acting alone, rapid production at 300 km from the relatively soft incident electron flux causes a rapid buildup of ionization above 250 km. Below 200 km equilibrium densities are reached after 10 min. Diffusion essentially drives O^+ ions away from steep density gradients, flattening the sharp density peak produced by local chemistry. As expected the chemistry and diffusion results are virtually identical at low altitudes (<200 km). Higher up, the density approaches equilibrium more rapidly with diffusion; the peak density is also slightly lower in altitude and only about 50% of the chemistry result. However, because of the flatter gradient, the O^+ density after 1 hr at 600 km is $3.2 \times 10^4 \text{ (cm}^{-3}\text{)}$ compared to 3.5×10^3 without diffusion.

Figures 4a-d show the effect of varying the high altitude O^+ flux from $1 \times 10^{12} \text{ m}^{-2} \text{ s}^{-1}$ (down) to -5×10^{12} (up). The differences are hardly noticeable until the critical outflow value is reached (Figure 4d), which has decreasing density above 400 km. After 10 min the diffusion speed is 100 m/s down in Figure 4a and 2 km/s up in Figure 4d.

D. Ionospheric Temperature

The thermal energy balance for ionospheric electrons is represented by a one dimensional, diffusion type equation (Hastings and Roble, 1977)

$$\frac{\partial E}{\partial t} = \frac{3}{2} n_e k \frac{\partial T_e}{\partial t} = \frac{1}{a} \frac{\partial}{\partial z} \left(a K_e \frac{\partial T_e}{\partial z} \right) + Q - L$$

(2.28)

E = energy density of thermal electrons (eV cm^{-3})

n_e = electron density (cm^{-3})

k = Boltzmann constant

K_e = thermal conductivity of the electron plasma ($\text{eV cm}^{-1}\text{s}^{-1} \text{K}^{-1}$)

a = cross sectional area of magnetic flux tube

Q, L = energy gain and loss rates, respectively ($\text{eV cm}^{-3} \text{s}^{-1}$)

The same Crank-Nicolson finite differencing scheme that solves for O^+ diffusion is used to solve the heat conduction equations. However, O^+ diffusion is relatively straightforward since the coefficients depend only on temperature and other parameters that are updated at regular time interval. Temperature, on the other hand, requires solving a non-linear equation with coefficients that depend on the temperature. With short time steps the problem is managed by assuring that coefficients change slowly enough to be linearly projected to the end of each time step. Alternatively, Hastings and Roble (1977) and Mantas et al. (1981) use Newton's method to solve a different formulation of the non-linear diffusion type, heat conduction equation.

Expanding (2.28)

$$\frac{\partial T_e}{\partial t} = b \left[K_e \frac{\partial^2 T}{\partial z^2} + \left(\frac{\partial K_e}{\partial z} + \frac{\partial a}{\partial z} K_e \right) \frac{\partial T_e}{\partial z} + Q - L \right] \quad (2.29)$$

$$b = 2/3n_e k.$$

In the form of (2.16) the coefficients are,

$$A = bK_e, B = b \left(\frac{\partial K_e}{\partial z} + K_e \frac{\partial a}{\partial z} \right), C = 0, D = Q - L.$$

The thermal conductivity given by Banks and Kockarts (1973), Vallance-Jones (1974) and others is expressed as

$$K_e = \frac{7.7 \times 10^5 T_e^{5/2}}{1 + 3.22 \times 10^4 \frac{T_e^2}{n_e m} \sum n_m Q D_k}$$

$$Q_{Dk} = \frac{1}{\frac{4}{3} \left(\frac{8kT_e}{\pi m_e} \right)^{1/2}} (v_e(N_2) + v_e(O_2) + v_e(O))$$

n_k = density of neutral species N_2 , O_2 , O (cm^{-3}).

Q_{Dk} involves collision frequencies of electrons with the neutral constituents, which in turn depend on T_e and n_k . The derivative of the flux tube area is calculated by assuming r^{-3} dependence for the cross sectional area of a dipole flux tube. In practice this modification turns out to be quite small, but it is retained for completeness.

The final term in (2.29) represents the net external source of heat given by the difference between heat generated by the electron flux and losses to the generally colder neutrals and ions. A normalized heat input from the electron flux transport code is multiplied by n_e to yield Q . Losses tabulated in Vallance-Jones (1974) are categorized as cooling by elastic collisions with neutrals and ions, cooling by rotational and vibrational excitations of N_2 and O_2 , and cooling by electronic excitations of O .

Within the program unit THERM in Figure 1, which shows the overall program logic, there are several subroutines needed to perform the temperature calculation. SETKE, which is executed only at the beginning of the program, sets up the altitude grid (now in 10 km steps from 130 to 600 km altitude) and initializes the temperature profile. If one selects the option to calculate electron temperature, the controlling routine ETEMP is called immediately after some input and initialization routines are run.

Because T_e can change rapidly from its initial profile, depending on conditions, the first time steps should be short (.05 - .1 s, e.g.). Temperature and densities at the beginning of the time step are used to compute coefficients in TECOEFF, which is called from the numerical solution routine, CONDTE. In a major departure from the

diffusion routine, coefficients values at the end of the time step are linearly extrapolated from the two previous time steps (except at $t=0$) to reflect potentially large changes in the coefficients. A quadratic extrapolation was also tried but the results did not differ appreciably from the linear version. Again, at the upper boundary the user has a choice between specifying a temperature or heat flux ($Q_n = -K_n \frac{\partial T_n}{\partial z}$, n =upper altitude index).

At the end of a time step DTTH, CONDTE returns control to ETEMP, which, after the first CONDTE call, reruns CONDTE with new time steps, $dt=DTTH/2$ and $dt=2 \times DTTH$. Results of this testing procedure are printed at the selected output times and allow the user to decide whether DTTH should be shortened or lengthened. Normally, ETEMP executes CONDTE until the end of an update interval, DTUP, is reached. Typical values for DTUP used in the examples range from .1s for $t < 1s$ to 5s for $t > 30s$. If the ion temperature option is also selected, similar routines are executed to calculate the ion temperature.

After the temperatures are calculated, O+ diffusion coefficients and chemical rate coefficients are recalculated using the new temperature profiles. The local chemistry and diffusion routines then run to find new densities at the end of the DTUP interval, after which the main program checks whether it is time to output results or end the model run. If neither condition is satisfied the program loops back for a new temperature calculation to the end of the next DTUP interval and so on. Because temperatures are computed first, rate coefficients for chemistry (constant throughout the DTUP interval) are based on temperatures at the end of the interval; thus the temperature is "ahead" of the density by the DTUP interval. Some form of averaging could minimize the discrepancy, but by keeping the DTUP interval relatively short compared to the time scale of density changes, .1-10s compared to several minutes in most cases, the mismatch should be negligible.

Because of the complexity of the model it is very difficult to make direct comparisons with measured temperatures. Although most results appear plausible, a real situation is usually much more dynamic than the constant flux assumed in the model; moreover, temperatures respond much more quickly to changes in flux input than densities, particularly in the F-region. Like diffusion, the high altitude heat flux is generally not available, although a high altitude temperature can be specified from measurements if desired.

Even though an analytic solution to the heat conduction equation with variable coefficients is not possible, a steady state solution with constant (in time) coefficients can be expressed as,

$$T(z) - T_1 = \int_{z_1}^z \frac{A_h p_h}{A(z')} dz' + \int_{z_1}^z \frac{1}{A(z')} \left(\int_{z_h}^{z'} S(z'') dz'' \right) dz' \quad (2.30)$$

z = altitude, z_1 = low altitude boundary, z_h = high altitude boundary

$$S(z) = -[Q(z) - L(z)], \quad p_h = \frac{\partial T}{\partial z} \quad \text{at } z_h.$$

A limited check of the Crank-Nicolson solution used in the model was carried out by stripping the temperature routines from the full code, running the reduced model to steady state, and comparing the results with a numerical integration (Simpson rule) of (2.30). Table 2 shows the results of one comparison. The table indicates that the model starts with T_e at about 2050 K at 600 km altitude, which then cools to about 1500 K after 960 s (ionosphere time). Analytic results using the same coefficients are nearly identical to the model results, giving some confidence that at least the numerical procedure is correct for a special situation with realistic temperatures. Although this check is a necessary condition for the validity of the model, it certainly is not a conclusive test under more realistic conditions.

3. Running the Ionospheric Chemistry Model

The growing complexity of the chemistry codes prompted the creation of setup programs that allow a knowledgeable user to more easily specify the numerous files and parameters required by the model program itself. Even with this aid the model cannot be called "user friendly", but the short preparatory codes and procedures do reduce the likelihood of typing errors and missing input files, permitting faster turn around especially when submitting similar jobs with varying input parameters. The various options and menus available are described in detail below.

The setup program runs in two parts; part 1 asks for input file names, output file names, and some processing options; part 2 allows one to change or accept parameters controlling boundary conditions, initial conditions, and output options. Once the selections are made, the ionospheric model can be either submitted as a batch job or run interactively at the terminal.

To run the programs a reasonably good working knowledge of the Cyber NOS-2 operating system is desirable and almost essential, particularly when problems occur, which inevitably happens. Procedures are used to automate the model as much as possible; these also require several indirect and direct access permanent files. The modified model codes are still written in FORTRAN version 4, as were the original codes. Since this version will eventually be unsupported they should be converted to the new standard, version 5. A conversion has been done but the compiled code took substantially more CPU time for execution in some cases. This problem may be connected with printing options, DO loop procedures or even the Post Mortem Dump utility, and until the exact solution is found it was decided to stay with a relatively efficient working code. The original documentation was adequate but spotty;

additional comments have been added at crucial points in the old code as well in the new or modified portions.

The chemistry model is started by typing and entering (RETURN) the Cyber procedure CHEM (on a permanent file with same name). A list of options then appears with brief descriptions. When satisfied with the option list, type and enter GO to begin a second procedure (BCHEMCZ) which contains the editing program for all model parameters. One can choose to edit a single group of parameters or the entire list. Depending on the selection, the current value of a parameter is displayed with the option to change or not; it is possible to go back and reedit any selection. Commonly used parameter sets can be saved on an indirect access permanent file which is specified as an option on the first setup program (FORMATTED FILE FOR CHEM-). The last used parameter set is also saved on a local file named PREV. Again, when satisfied with the parameter settings, type GO to submit the model as a batch or interactive job.

A. First List (Options, LIST=PART)

After typing and entering CHEM a list of options with the current settings appears; the choices can be grouped in the categories of input file, output files, and processing options.

1. Input files

PRFILE - Production rate file created by the electron flux transport (B3C) and production rate codes (PRATES) executed in the TRAN procedure. This file contains the altitude grid, neutral atmosphere model, production rate profiles, and the normalized electron plasma heating rate; enter this file name without the PR prefix.

INITIAL ION DENSITY - A deck name in the DATAPL (UPDATE utility) file denoting a file that contains specified initial density profiles of selected ions.

NEUTRAL ATM. MODEL - A deck name in the DATAPL file that contains the appropriate neutral atmosphere model; this is not used if the neutral atmosphere model from the PRFILE is specified from the parameter list (below).

ALTERNATE INITIAL DEN FILE - A file (OUTPUT FILE (ALL DENSITIES)) created by a previous chemistry run, containing density and temperature profiles at the last output time, that can be used in place of the file designated by INITIAL ION DENSITY. This is useful if initial densities based on a particular flux are desired, for example a relatively steady flux that produces a background ionosphere.

2. Output files

PLOTFILE (DEN., TEMP., ELEC. COND.) - A file, used by plotting programs, that contains calculated electron and O+ density profiles, as well as electron temperature, ion temperature, and the Hall and Pedersen electric conductivities. Data is collected at output times specified by the user in the parameter list. A FORTRAN plotting routine on the Cyber has been developed (PLTESTP for pen plots), or, for interactive plots on the screen, there are ZBASIC programs (with special IGL plotting commands) for the Zenith Z-100 personal computer.

OUTPUT FILE (ALL DENSITIES) - A file containing all density and temperature profiles generated at the last output time for the run. This is the ALTERNATE INITIAL DEN FILE specified by a later run if one wished to use these profiles as initial conditions.

2 Processing options

(B)ATCH OR (I)NTERACTIVE JOB - Enter B for a batch job that is routed to the input queue for execution; enter I for immediate interactive execution. Interactive jobs are useful for testing because execution usually starts

immediately, although the users terminal session is tied up until completion (unless the job is detached). Batch processing is generally desirable for routine runs because multiple runs can be submitted and the terminal is freed up.

PARAMETER FILE - a file containing the parameters that can be edited (below). Normally this is the DCPL file associated with the BCHEMED procedure; however, another file in the same format can be substituted.

BATCH ROUTE CODE (IN,TO) - a parameter designating whether the printed model output appears on the OUTPUT (select IN) file printed at the computer center or on a wait file which can be accessed at the terminal by a QGET command (select TO). TO is the normal choice since the user can quickly check the results, which can be ROUTED to a line printer using the DC=PR option. The output file is usually too long to be printed locally, but it can be edited so that portions may be printed, if desired.

SEQUENCE NO. (DEFAULT=1) - If multiple batch jobs are submitted each run must have a distinct sequence number so that each will access the correct files.

The following items are listed only if the LIST=ALL parameter is explicitly set when the CHEM procedure is invoked. Most are relevant only for development purposes and should be changed only if the user is familiar with the programs and procedures.

RATE COEFF CORRECTION FILE - an UPDATE correction file that contains modified and additional chemical reactions pertinent to ionospheric chemistry (collected from Vallance-Jones, 1977). The default setting is PICORR.

FTH (THERMAL CODE SUFFIX) - a character used to specify the file containing the temperature subroutines. The default setting is 4.

FEL (ELEC. COND. CODE SUFFIX) - a character used to specify the file containing the electric conductivity subroutines. The default setting is Y.

PRFILE FROM OLD(0) OR NEW(1) CODE - choice determines whether PRFILE format is that generated by original FORTRAN 4 code or revised FORTRAN 5 version. The default is 0, designating the FORTRAN 4 version.

NEW COMPILATION (Y,N) - choice determines whether previously compiled model code is executed (N), or new source code is to be compiled before execution. The default setting is N.

OPTICS (Y,N) - choice determines whether file containing source code for calculation of optical emissions is merged with main chemistry code before compilation (relevant only if Y is selected for NEW COMPILATION option, above). The default setting is Y.

CHEM PROCEDURE VERSION - a character suffix specifying the file containing the procedure that executes the ionospheric chemistry model. The default setting is 4.

PROGRAM STOP PARAMETER - a number allowing a programmer to stop model execution at a desired point in the code by inserting STOP statements in a modified source code. The default setting is 0.

B. Second list

After the editing program is loaded the main list appears:

A. INITIAL DENSITY FILES

B. MAIN CHEM OPTIONS

C. DIFFUSION ALT. GRID

D. TE,TI UPPER ALT. FLUXES

E. CHEM TIME STEPS

F. SCALE FACTORS

G. O+ UPPER ALT. FLUX

H. DIFFUSION,TEMP. PARAMETERS AND OUTPUT OPTIONS

I. DISPLAY ALL CHOICES (A-I)

ENTER SELECTION A-I

OR TYPE GO TO RUN WITH CURRENT PARAMETERS

After making a selection a group of parameters (from the DCPL file specified in the first list) is displayed along with the option of making a change or letting them stand. When satisfied with the displayed parameters the user can return to the main list and choose another group to edit or enter GO to submit the job for execution. Usually after an incorrect response the CHANGE(Y/N)? prompt reappears. If a mistake is made in entering data it can be edited again, or if hopelessly lost, the CONTROL-T abort combination can be entered to leave the procedure and return to the NOS backslash prompt (\), after which the CHEM procedure can be tried again. After entering GO from the main list or the H option, the status report INPUT FILE WRITTEN appears along with a listing of the batch job file (if selected) that will be routed. The job is then routed and the status after submission (INPUT QUEUE or EXECUTING, e.g.) is listed on the screen. If the interactive option is chosen from the CHEM argument list the job will run until the EXIT response signals the job has finished. While the job is running one can enter ESC(APE) and then enter E to get a status report. Model output from an interactive job will be on the local file OUTPR.

4. Parameterization of the Flux Transport Model

A. Motivation

Besides the inherent complexity of the ionospheric chemistry model, the code requires many parameters and external inputs. For example, there are initial and boundary conditions, a background neutral atmosphere, and production of various atomic and molecular species as well heat generated by incident electrons, protons, or solar radiation. In many situations these parameters do not change, but particle fluxes are often highly dynamic and spatially nonuniform, especially near auroral arcs. Since the models (production rates and chemistry) are one dimensional along a magnetic field line, they do not account for horizontal transport produced by electric fields. However, the models could be run with fluxes measured at various points across the arc, and, by combining the measured electric field with the calculated horizontal density gradient, an additional source term could be included in the chemical rate equations. Similarly, a time dependent flux could be simulated by inserting different production rates at appropriate times in the chemistry calculations.

The calculation of production rate profiles by an incident particle flux alone is a complicated task. There are semi-empirical, range theoretic models (e.g., Rees (1963; Roble and Rees (1977)) and quantitative models based on the Boltzmann equation and cross sections for ionization and excitation (Strickland, 1976; Banks et al., 1974; Mantas et al., 1975). We have applied the Strickland model to studies of polar cap auroral arcs (Weber et al., 1988). Production rates calculated for the maximum electron flux measured by a rocket over an arc were input to the ionospheric chemistry model described above. Since the models (flux transport and chemistry) are one dimensional along a magnetic field line, they do not account for horizontal transport

produced by electric fields. However, the models could be run with fluxes measured at various points across the arc, and, by combining the measured electric field with the calculated horizontal density gradient, an additional source term caused by $E \times B$ convection could be included in the chemical rate equations.

A need for production rate profiles corresponding to many different fluxes is restrictive because of the large computational expense involved. Aside from multiplication by a constant factor or a simple time dependence, there has been no alternative to a new run of the flux transport code for each unique flux. We have found, however, that production rate profiles can be quickly approximated by scaling a table of rate profiles calculated for a specified unit flux over a grid of discrete energies. We will describe below how the tables are generated along with several examples.

B. Outline of Strickland Flux Transport Model

The Boltzmann equation for electrons

$$\frac{\partial f}{\partial t} + \mathbf{v} \cdot \nabla_r f + \mathbf{a} \cdot \nabla_v f = \frac{\partial f}{\partial t}_{\text{coll}}$$

(4.1)

is reduced to an equation of transfer with azimuthal symmetry about geomagnetic field lines,

$$\mu \frac{\partial \phi(\tau, E, \mu)}{\partial t} = -\phi(\tau, E, \mu) + \sum_k r_k(E, \tau) \int R_k(\mu', \mu, E', E) \phi(\tau, E', \mu') dE' d\mu'$$

(4.2)

ϕ = flux ($\text{cm}^{-2} \text{ s}^{-1} \text{ sr}^{-1} \text{ eV}^{-1}$), R_l = redistribution function

μ = cosine pitch angle, k corresponds to neutral constituent species (N_2 , O_2 ,

O)

τ = scattering depth, $d\tau = \sum_k n_k(z) \sigma^k(E) dz$, n_k = neutral density, z = altitude

σ^k = total cross section for all scattering processes

$r^k = n_k(z) \sigma^k(E) / \sum_i n_i(z) \sigma^i(E)$

This form of the Boltzmann equation is one dimensional and neglects any forces, e.g., electric fields, along magnetic field lines. This permits the model to step successively from higher to lower energies since an electron can only change direction by elastic scattering or lose energy by ionization or excitations of the neutral constituents.

A matrix representation of the equation of transfer is then derived over a 2-dimensional grid of energies and pitch angles. The coefficients are obtained by assuming that the flux within each grid cell can be approximated by a function quadratic in $\log(E = \text{energy})$ and linear in μ . A power law continues the flux beyond the highest grid energy. At each energy the flux is given by

$$\mu_i \frac{\partial \phi_i(\tau, E, \mu)}{\partial \tau} = -\phi_i + \sum_k r_k \sum_j A_{kj}^k \phi_j + S_i' \quad (4.3)$$

i, j indices range over pitch angle; n, m range over energy.

$S_i' = \sum_k r_k \sum_{j, n < m} A_{nmij} \phi_{mj}$ = source function from higher energies.

An eigenvalue solution of the matrix equation is calculated at an intermediate altitude of the altitude range. The high altitude incident flux constitutes one boundary condition; zero upward flux at the lowest altitude completes the necessary boundary conditions. Differential flux solutions at other altitudes are approximated by an iterative method. Finally, the computed profile of

differential electron flux is integrated over pitch angle and input to a production rate code that yields production rate profiles of 14 ionic and neutral species.

The principal requirements of the model are:

- (1) Tables of ionization and excitation cross sections for electrons colliding with N_2 , O_2 , and O .
- (2) A neutral atmosphere model with densities of N_2 , O_2 , and O . The examples below use a Jacchia 1977 model having 1000 K exospheric temperature.
- (3) Specified energy and pitch angle grids. Since we are mainly concerned with soft electron fluxes often observed over polar cap auroral arcs, typically having energies around a few hundred eV, we use 19 transport energies ranging from 1800 eV to 10 eV and 7 energies from 8 eV to 3 eV which are deposited locally. 20 pitch angles, 10 each over the up- and downgoing hemispheres are standard.
- (4) A differential flux at the grid energies and pitch angles incident at the upper boundary. The examples assume a downgoing isotropic flux at 450 km altitude, near the altitude of rocket observations in recent AFGL experiments (PIIE, Polar Arcs).

C. Constructing the Tables

When results for different incident fluxes incident on the same neutral atmosphere are desired, computations involving (1), (2), and (3) above are duplicated. Because each transport run needed to calculate a flux profile can take nearly 2 min CPU on a Cyber 760 computer, situations where dozens of runs are required may consume excessive amounts of machine time. Execution time can be shortened considerably by determining the contribution to production by a unit flux at each grid energy. Multiplying each contribution by the actual flux at that energy scaled to the unit flux yields the contribution

by that flux. Final rate profiles are produced by adding the contributions from all energies. A complete set of rate profiles from a single differential flux spectrum can be generated in 1 s of CPU time.

Although ultimately there may be better ways to do the job, Figure 5 illustrates how to construct the tables. This schematic shows how the contributions from energy E_5 is found. Spectrum 4 (S_4) represents a transport and production run yielding production rate profiles F_4 for a constant incident flux ϕ_1 up to E_4 and a lower flux ϕ_0 at higher energies on the grid. ϕ_1 is comparable to the level of a realistic flux, ϕ_0 is low enough to add essentially no production compared to ϕ_1 . In the examples below $\phi_1 = 1 \times 10^5$, $\phi_0 = 1 \times 10^0$. S_5 is similar to S_4 but ϕ_1 extends to E_5 . By subtracting the production rate profiles generated by S_4 from the corresponding profiles generated S_5 , one is left with the production by ϕ_1 at E_5 . Subtracting neighboring pairs of runs at the other grid energies completes the table of contributions from all energies except one (the lowest transporting energy).

A range of 20 energies, for example, still requires 20 full transport runs to construct a full table. This also demands considerable computer time; the tables would be justified only when a relatively large number of fluxes is encountered, such as when modelling detailed behavior across an auroral arc or in global 3-D ionospheric simulations. Global modelling would require a table for each neutral atmosphere, but careful interpolation may lessen the need for many such table. Similarly, each pitch angle dependence, isotropic, beamlike, or conic would demand its own table.

The time to generate a table can be further shortened by considering some details of the code logic. Namely, (1) eigenvalues need not be recalculated for each run, and (2) source functions and flux results at higher energies can be

saved and reused for subsequent runs at lower energies. These savings could reduce the time to construct tables by 50%.

D. Results and Examples

Figures 6a-f are plots of tabular rate profiles of 3 ionic species for selected energies ranging from 55 to 1300 eV in response to isotropic incident flux of electrons, $\phi_1 = 1 \times 10^5 \text{ (cm}^{-2} \text{ s}^{-1} \text{ sr}^{-1} \text{ eV}^{-1})$ at each energy. The altitude of peak production ranges from over 300 km at 55 eV to 150 km at 1300 eV; peak rates range from 10^{-1} to $10^2 \text{ (cm}^{-3} \text{ s}^{-1})$. Note that the production rate scale changes at higher energies.

To compare table results with a full electron transport and production run, a flux spectrum from the AFGL PIIE experiments, Figure 7a, was input to the full code. Figure 7b shows production rates from the tables using the flux in Figure 7a. Table 3 compares rates scaled from the tables with those from the full code (shown in parentheses when different). It is evident that most table results are very close to the full model values. Profiles generated from the tables for a 200 eV Maxwellian flux (Figure 8a) are plotted in Figure 4b. The type of agreement is similar to that seen in Table 3.

Work remains to explore where and why discrepancies exist and to place limits on the types of fluxes the method is able to handle. The examples above and Maxwellian fluxes at 80 and 600 eV (not shown) indicate that the tables perform well for reasonably behaved fluxes. Further tests are needed for higher energy auroral precipitation at several keV and for more unusual fluxes, e.g., double peaks. A cursory glance at Table 3 and the other species suggests that the ionic production rates compare better than some neutral excited species. Thus, the table may be better suited for studies involving total ion density rather than excited states.

As indicated earlier, auroral arc modelling could be an immediate beneficiary of the tabular production rates. The inherent one dimensional nature of the transport model, however, assumes horizontal uniformity and limits the resolution of a structure to scales greater than an electron gyroradius. This is not a serious concern for arcs several tens of kilometers across. The tables will permit much more experimentation with spatial structure and time dependence to simulate the increasingly detailed observations provided by radars and photometers.

Finally, a longer term goal would be to set up a data base of lookup tables for users to access production rates for a wide variety of neutral atmospheres, incident altitudes, and pitch angle dependences. Several altitudes may be required to accommodate rocket, satellite, or magnetospheric model inputs. Global modelling demands the widest range of possibilities, but could gain considerably by refining the cruder zonal inputs now used.

5. PIIE Results

Figure 9 displays measurements taken by the instrumented rocket payload as it passed over a complicated system of F-layer auroral arcs near apogee. The vertical line indicates the time chosen for model comparisons. The electron density had a local maximum of $3 \times 10^4 \text{ cm}^{-3}$ and T_e was about 3000 K at 415 km altitude. Electrons precipitating into the arc carried an energy flux of about .1 ($\text{erg cm}^{-3} \text{ s}^{-1}$), nearly an order of magnitude greater than in adjacent regions. A Jacchia 1977 neutral atmosphere model with 1000 K exospheric temperature was employed. Densities at 450 km and 105 km altitude for N_2 , O_2 , and O range from 1.3×10^6 to $3.9 \times 10^{12} \text{ cm}^{-3}$, 2.9×10^4 to $7.7 \times 10^{11} \text{ cm}^{-3}$, and 4.7×10^7 to $3.2 \times 10^{11} \text{ cm}^{-3}$, respectively. Energy transfer from the energetic electrons to ambient thermal electrons are based on expressions given by Schunk and Hays (1971).

Figure 10 shows direct production rates for three major ions and the heating rate resulting from the precipitating flux marked 282.3-288.1 s in Figure 11. This 10 point average sample describes conditions near the center of the arc. The model energy grid has 19 transporting energies from 1800 eV to 10 eV and 7 non-transporting energies from 9 eV to 3 eV. Electrons in the non-transporting energy range are assumed to deposit their energy locally. Fluxes at energies greater than 1800 eV are continued with a power law dependence to 5 keV. Electrons at the high altitude boundary are assumed to be isotropic over the upper hemisphere; zero upward flux through the lower boundary at 105 km altitude completes the boundary conditions. Curves (a) and (b) in Figure 10 refer to normalized heating rates corresponding to the two ambient electron density profiles (constant in time, cf. Figure 12). Differences in production rates for the assumed profiles are less than 1%. Energy conservation tests, which compare the net energy into the column

with that expended in ionization and excitation, agree within 6% for case (a) and 2% for case (b).

Chemistry model results over a 5 min interval using production rates calculated for the flux inside the arc are shown in Figure 12. The initial electron density profile at $t=0$ is a model calculation with a representative flux near the arc shown in Figure 11. Also indicated in Figure 12 are the ambient electron density profiles referred to in Figure 10. Although the model is internally self-consistent the normalized heating rate and production rates are held constant during the calculation. Since Figure 10 indicates that the heating rate depends significantly on the electron density, the corresponding T_e profiles are markedly different; the electron density profiles, however, are more nearly alike (2-4% in the F-region, 6-10% in the E-region) and are not shown in the figure for clarity. Electric conductivities (Figure 13) are determined from expressions given in Vallance-Jones (1974). Height integrated Pedersen conductivity at 5 min range from .76 to .80 (mho m^{-1}) using curves (b) and (a), respectively.

Electron densities after 2-5 min in Figure 12 approximate the measured values at 400 km altitude; model T_e , however, is 600-1000 K less than measured. Although F-region densities increase rapidly there is little change at lower altitudes. This is a response to the large increase in flux at energies less than 1 keV; fluxes at energies greater than 1 keV are very similar both inside and outside the arc. Even if the 15 s profile were taken as the initial condition, when F-region densities were nearly ten times greater than at $t=0$, the final profile after several minutes have passed would be nearly identical.

Although the model electron density compares reasonably well with the data, the electron temperature agreements is less satisfactory. Because the only source now incorporated in the model is collisional heating by energetic

electrons, this discrepancy may in part stem from other types of heating. More fundamentally, heat conduction is only part of the full energy balance equation (Schunk and Walker, 1970); terms representing other forms of heat transport could modify the results. For example, Schunk et al. (1986) demonstrate that thermoelectric cooling by field-aligned currents becomes significant only for rather large return currents of thermal electrons on the order of $10 \mu\text{A m}^{-2}$. Weber et al. (1988) estimate maximum field-aligned currents of about $5 \mu\text{A m}^{-2}$ within the arc, suggesting a minimal contribution from this effect.

Densities associated with an arc lasting a few minutes to several tens of minutes depend both on the initial ionosphere and the duration of enhanced production. Although direct production by precipitating electrons leads to a rapid buildup of ionization, equilibrium resulting from chemistry and diffusion is reached slowly (several tens of minutes in the F-region vs. minutes in the E-region). Starting with rather artificial initial conditions, the next two examples (Figures 14 and 15) illustrate how the electron density profile develops when a flux like that observed during PIIE is turned on continuously for 30 minutes.

In Figure 14, O^+ ions alone are present initially with a constant height profile of 10^4 cm^{-3} . From 120 to 200 km altitude production and loss quickly balance and equilibrium densities are reached after 10 minutes or so. Below 120 km production is slight and the density actually decreases. Ion production dominates above 200 km, causing a steady increase in electron density that is limited by O^+ diffusion until equilibrium is reached several hours later. Starting with an O^+ density of 10^3 cm^{-3} , Figure 15 indicates that the final density profile after 30 minutes is not different than seen in Figure 14, except at the lowest altitudes. From 130 to 200 km the equilibrium densities are nearly

equal; above 200 km the profiles are similar but lag behind those in Figure 14 because of the smaller initial density. However, on time scales longer than 5 minutes, the resulting densities above 100 km agree to within 20% even when drastically different initial conditions are assumed.

Figure 16 shows what happens if the flux is turned on for 15 minutes and then suddenly switched off, after which direct production ceases and ionization decays, subject only to local chemistry and diffusion. Following an abrupt drop caused by rapid losses, the electron density slowly decays, especially at and above the altitude peak. Diffusion flattens the profile and maintains the density above 400 km where losses by recombination are minimal.

For comparison, Figures 17 and 18 show electron density profiles generated by fluxes measured outside the main auroral arc. Initial O⁺ densities are 10^4 and 10^3 cm^{-3} as before. Here the initial density conditions clearly affect the profiles even after several minutes have elapsed. Only in the E-region where local chemistry is relatively fast do the densities approach the same equilibrium, and neither case approximates the densities observed in the downleg segment. Since the electron energy flux measured from 420 km to 290 km nowhere approaches the more energetic flux seen earlier, it seems likely that the observed electron density results from a combination of ionization remaining after local production ceased and that brought in by convection.

A future goal of this study is to find the relationship between large scale features in the polar cap ionosphere and scintillations of satellite to ground radio transmissions. Scintillations are caused by plasma density irregularities with scale sizes from 100 m to 10 km (Weber and Buchau, 1985). These irregularities have been associated with plasma instabilities generated by density gradients in enhanced plasma regions (blobs) hundreds of kilometers

across or with velocity shears (Basu et al., 1986). Hence, density features resulting from direct production or transport play an important role in the problem. For example, observed changes in scintillation behavior with the solar cycle (Aarons, 1982) may be connected with the way these features are generated. A model can probe how similar fluxes affect neutral atmospheres with different exospheric temperatures. In Figure 19, a cold atmosphere like that found during solar minimum produces a slightly higher density at lower altitudes. A hot neutral atmosphere has peak density above 300 km and a more gradual decrease toward higher altitudes (Figure 20). Differences between profiles may help identify which processes generate irregularities and the scale sizes likely to be observed.

References

Aarons, Jules, Global morphology of ionospheric scintillations, Proc. IEEE, **70**, 360, 1982.

Banks, P.M., and G. Kockarts, Aeronomy, Part B, Academic Press, New York, 1973.

Banks, P.M., Chapell, C.R., and A.F. Nagy, A new model for the interaction of auroral electrons with the atmosphere: spectral degradation, backscatter, optical emission, and ionization, J. Geophys. Res., **79**, 1459, 1974.

Basu, Sunanda, Basu, Santimay, Senior, C., Weimar, D., Nielsen, E., and P.F. Fougere, Velocity shears and sub-km scale irregularities in the nighttime auroral F-region, Geophys. Res. Lett., **13**, 101, 1986.

Gerald, Curtis, F., and Patrick O. Wheatley, Applied Numerical Analysis, Third edition, Addison-Wesley Publishing Co., Reading, MA, 1984.

Hastings, J.T., and R.G. Roble, An automatic technique for solving coupled vector systems of non-linear parabolic partial differential equations in one space dimension, Planet. Space Sci., **25**, 209, 1977.

Jones, R.A., and M.H. Rees, Time dependent studies of the aurora 1. ion density and composition, Planet. Space Sci., **21**, 537, 1973.

Mantas, George P., Carlson, Herbert C. Jr., and Caesar H. LaHoz, Thermal response of the F region ionosphere in artificial modification experiments by hf radio waves, J. Geophys. Res., **86**, 561, 1981.

Mantas, George P., and James C.G. Walker, The penetration of soft electrons into the ionosphere, Planet. Space Sci., **24**, 409, 1975.

Roble, R.G., and M.H. Rees, Time-dependent studies of aurora: effects of particle precipitation on the dynamic morphology of ionospheric and atmospheric properties, Planet. Space Sci., **25**, 991, 1977.

Rees, M.H., Auroral ionization and excitation by incident energetic electrons, Planet. Space Sci., **11**, 1209, 1963.

Schunk, Robert W., and Paul B. Hays, Photoelectron energy losses to thermal electrons, Planet. Space Sci., **19**, 113, 1971.

Schunk, Robert W., and James C.G. Walker, Thermal diffusion in the F2-region of the ionosphere, Planet. Space Sci., **18**, 535, 1970.

Schunk, R.W., Sojka, J.J., and M.D. Bowline, Theoretical study of the electron temperature in the high-latitude ionosphere for solar maximum and winter conditions, J. Geophys. Res., **92**, 6013, 1987.

Strickland, K.J., Book, D.L., Coffey T.P., and J.A. Fedder, Transport equation techniques for the deposition of auroral electrons, J. Geophys. Res., 81, 2755, 1976.

Vallance Jones, Alister, Aurora, D. Reidel Publishing Co. Inc., Boston, 1974.

Weber, E.J., and J. Buchau, Observations of plasma structure and transport at high latitudes, in The Polar Cusp, p.279, ed. by J.A. Hottel and A. Egeland, D. Reidel Publishing Co. Inc., Boston, 1985.

Weber, E.J., Tsunoda, R.T., Buchau, J., Sheehan, R.E., Strickland, D.J., Whiting, W., and J.G. Moore, Coordinated Measurements of auroral zone plasma enhancements, J. Geophys. Res., 90, 6497, 1985.

Weber, E.J., Kelley, M.C., Ballenthin, J.O., Basu, S., Carlson, H.C., Fleischman, J.R., Hardy, D.A., Maynard, N.C., Pffaf, R.F., Rodriguez, P.A., Sheehan, R.E., and M. Smiddy, Rocket measurements within a polar cap arc: plasma, particle, and electric circuit parameters, J. Geophys. Res., in press, 1988.

Table 1

Chemical reactions used in the ionospheric chemistry model (taken from the model input file). Reactions are grouped by production and loss for each species. Rates equal to -1.00E 00 indicate T_e dependence interpolated from a separate table. Reactions with asterisks indicate additions or modifications to the original set.

Rate				Reaction			
NO+							
10 01							
PROD							
13 03	-1.00E 00	02 1.00	N2+	+ O	---->	NO+	+ N
12 02	2.00E-10	00	N+	+ O2	---->	NO+	+ N
06 01	5.00E-16	00	O2+	+ N2	---->	NO+	+ NO
06 08	4.40E-10	00	O2+	+ NO	---->	NO+	+ O2
06 09	1.80E-10	00	O2+	+ N	---->	NO+	+ O
07 01	-1.00E 00	01 1.00	O+	+ N2	---->	NO+	+ N
12 08	8.00E-10	00	N+	+ NO	---->	NO+	+ N
13 08	3.30E-10	00	N2+	+ NO	---->	NO+	+ N2
07 08	-1.00E 00	18 1.00	O+	+ NO	---->	NO+	+ O
14 08	1.20E-09	00	O+(2D)	+ NO	---->	NO+	+ O
LOSS							
0.00E 00 SPONTANEOUS DECAY RATE							
05 04	-1.00E 00	03	NO+	+ EL	---->	N	+ O
O2+							
05 05							
PROD							
12 02	4.00E-10	00	N+	+ O2	---->	O2+	+ N
07 02	-1.00E 00	05 1.00	O+	+ O2	---->	O2+	+ O
13 02	-1.00E 00	04 1.00	N2+	+ O2	---->	O2+	+ N2
14 02	1.00E-10	00	O+(2D)	+ O2	---->	O2+	+ O
15 02	3.00E-10	00	O+(2P)	+ O2	---->	O2+	+ O
LOSS							
0.00E 00							
06 01	5.00E-16	00	O2+	+ N2	---->	NO+	+ NO
06 08	4.40E-10	00	O2+	+ NO	---->	NO+	+ O2
06 09	1.80E-10	00	O2+	+ N	---->	NO+	+ O
06 10	4.00E-10	00	O2+	+ N(2D)	---->	N+	+ O2
06 04	-1.00E 00	06	O2+	+ EL	---->	O	+ O

05 04-1.00E 00 03 0.20	NO+	+	EL	----	N	+	O
12 03 2.20E-12 00	N+	+	O	----	N	+	O+
12 08 8.00E-10 00	N+	+	NO	----	N	+	NO+
10 01 1.60E-14 00	N(2D)	+	N2	----	N	+	N2
10 03 2.00E-13 00	N(2D)	+	O	----	N	+	O
10 04-1.00E 00 12 1.00	N(2D)	+	EL	----	N	+	EL
19 03 5.00E-11 00	N2(A3S)	+	O	----	N	+	NO
LOSS							
0.00E 00							
09 02-1.00E 00 11	N	+	O2	----	NO	+	O
09 08-1.00E 00 10	N	+	NO	----	N2	+	O
09 06 1.20E-10 00	N	+	O2+	----	NO+	+	O
O+							
07 05							
PROD							
14 03 0.00E-11 00	O+(2D)	+	O	----	O+	+	O
14 04-1.00E 00 09 0.50	O+(2D)	+	EL	----	O+	+	EL
15 04-1.00E 00 09 0.50	O+(2P)	+	EL	----	O+	+	EL
13 03-1.00E 00 07 1.00	N2+	+	O	----	O+	+	N2
12 03 2.20E-12 00	N+	+	O	----	O+	+	N
12 02 2.00E-11 00	N+	+	O2	----	O+	+	NO
14 01 2.00E-11 00	O+(2D)	+	N2	----	O+	+	N2
LOSS							
0.00E 00							
07 01-1.00E 00 01	O+	+	N2	----	NO+	+	N
07 02-1.00E 00 05	O+	+	O2	----	O2+	+	O
07 08-1.00E 00 18	O+	+	NO	----	N+	+	O2
07 10 1.30E-10 00	O+	+	N(2D)	----	N+	+	O
07 04 1.60E-12 00	O+	+	EL	----	O	+	(7774A)
NO							
00 01							
LOSS							
0.00E 00							
08 06 0.00E 00 00							
N(4S)							
11 03							
PROD							
13 04-1.00E 00 08 1.00	N2+	+	EL	----	N	+	N(2D)
13 03-1.00E 00 02 0.05	N2+	+	O	----	N	+	NO+
12 02 3.00E-10 00	N+	+	O2	----	N	+	O2+
07 01-1.00E 00 01 1.00	O+	+	N2	----	N	+	NO+

```

N(2D)
05 07
PROD
13 04-1.00E 00 08 1.00 N2+ + EL ----> N(2D) + N
13 03-1.00E 00 02 0.95 N2+ + O ----> N(2D) + NO+
12 02 3.90E-10 00 N+ + O2 ----> N(2D) + O2+
05 04-1.00E 00 03 0.80 NO+ + EL ----> N(2D) + O
19 03 5.00E-11 00 N2(A3S) + O ----> N(2D) + NO
LOSS
1.10E-05
10 01 1.60E-14 00 N(2D) + N2 ----> N + N2
10 02-1.00E 00 19 N(2D) + O2 ----> N + O2
10 08 7.00E-11 00 N(2D) + NO ----> N + NO
10 06 4.00E-10 00 N(2D) + O2+ ----> N+ + O2
10 03 4.00E-13 00 N(2D) + O ----> N + O
10 04-1.00E 00 12 N(2D) + EL ----> N + EL
10 07 1.30E-10 00 N(2D) + O+ ----> N+ + O
O2(1DELG)
00 03
LOSS
3.70E-04
11 09-1.00E 00 13 O2(1DG) + N ----> O2 + N
11 03 1.00E-17 00 O2(1DG) + O ----> O2 + O
11 02-1.00E 00 14 O2(1DG) + O2 ----> O2 + O2
N+
02 05
PROD
06 10 4.00E-10 00 O2+ + N(2D) ----> N+ + O2
07 10 1.30E-10 00 O+ + N(2D) ----> N+ + O
LOSS
0.00E 00
12 02 2.00E-11 00 N+ + O2 ----> O+ + NO
12 02 2.00E-10 00 N+ + O2 ----> NO+ + O
12 02 4.00E-10 00 N+ + O2 ----> O2+ + N
12 03 2.20E-12 00 N+ + O ----> O+ + N
12 08 8.00E-10 00 N+ + NO ----> NO+ + N
N2+
03 05
PROD
16 01 2.50E-10 00 O2+(A4P) + N2 ----> N2+ + O2
14 01 1.00E-10 00 O+(2D) + N2 ----> N2+ + O
15 01 4.80E-10 00 O+(2P) + N2 ----> N2+ + O
LOSS
0.00E 00
13 02-1.00E 00 04 N2+ + O2 ----> O2+ + N2
13 03-1.00E 00 02 N2+ + O ----> NO+ + N(2D)
13 08 3.30E-10 00 N2+ + NO ----> NO+ + N2
13 04-1.00E 00 08 N2+ + E ----> N + N
13 03-1.00E 00 07 1.00 N2+ + O ----> O+ +N2

```

```

O+(2D)
00 05
LOSS
7.70E-05
14 01 1.00E-10 00 O+(2D) + N2 ----> N2+ + O
14 02 1.00E-10 00 O+(2D) + O2 ----> O2+ + O
14 03 0.00E-11 00 O+(2D) + 0 ----> O+ + O
14 04-1.00E 00 09 O+(2D) + EL ----> O+ + EL
14 08 1.20E-09 00 O+(2D) + NO ----> NO+ + O
O+(2P)
00 03
LOSS
2.00E-01
15 01 4.80E-10 00 O+(2P) + N2 ----> N2+ + O
15 02-1.00E 00 05 O+(2P) + O2 ----> O2+ + O
15 04-1.00E 00 09 O+(2P) + EL ----> O+ + EL
O2+(A4PI)
00 04
LOSS
0.00E 00
16 01 2.50E-10 00 O2+(A4P) + N2 ----> N2+ + O2
16 02 3.00E-10 00 O2+(A4P) + O2 ----> O2+ + O2
16 03 1.00E-10 00 O2+(A4P) + O ----> O+ + O2
16 04 1.00E-07 00 O2+(A4P) + EL ----> O + O
O(1D)
05 03
PROD
10 08 2.00E-11 00 N(2D) + NO ----> O(1D) + N2
10 03 2.00E-13 00 N(2D) + O ----> O(1D) + N
10 02 4.80E-12 00 N(2D) + O2 ----> O(1D) + NO
06 04-1.00E 00 06 1.00 O2+ + E ----> O(1D) + O
18 03-1.00E 00 20 2.00 O(1S) + O ----> O(1D) + O(1D)
LOSS
6.74E-03
17 01 2.30E-11 00 O(1D) + N2 ----> O + N2
17 08 3.50E-11 00 O(1D) + NO ----> O + NO
17 02 4.10E-11 00 O(1D) + O2 ----> O + O2
O(1S)
04 04
PROD
12 02 1.90E-10 00 N+ + O2 ----> NO+ + O
06 04-1.00E 00 06 0.08 O2+ + E ----> O(1S) + O
19 03 3.60E-11 00 N2(A3S)(1)+ + O ----> O(1S) + N2
06 09 2.50E-11 00 O2+ + N(4S) ----> O(1S) + NO
LOSS
1.41E 00
18 03 2.00E-14 00 O(1S) + O ----> O(1D) + O(1D)
18 08-1.00E 00 15 O(1S) + NO ----> O + NO
18 02-1.00E 00 16 O(1S) + O2 ----> O + O2
18 11 1.70E-10 00 O(1S) + O2(1DG) ----> O + O2

```

N2(A3SIG)

00 04

LOSS

5.30E-01

19 02 2.00E-11 00

19 03 3.40E-11 00

19 08 4.00E-11 00

19 09 5.00E-11 00

O2(B1SIG)

01 02

PROD

17 02 5.00E-11 00

LOSS

8.30E-02

20 02-1.00E 00 17

20 01 1.00E-17 00

N2(A3S) + O2

N2(A3S)(1)+ O

N2(A3S)(1)+ NO

N2(A3S) + N

----> N2 + O2

----> N2 + O

----> N2 + NO

----> N2 + N

O(1D) + O2

----> O + O2(B1S)

O2(B1S) + O2

----> O2 + O2

O2(B1S) + N2

----> O2 + N2

Table 2

Comparison of model T_e with analytic expression (both at steady state).

ALT	initial T_e (K)	A	S	model T_e (K)	analytic T_e (K)
600	2048	1.46(14)	7.20(0)	1494	1495
500	2048	1.46(14)	5.10(1)	1488	1489
450	2033	1.44(14)	1.02(2)	1474	1475
400	2004	1.38(14)	1.69(2)	1441	1442
350	1941	1.28(14)	2.26(2)	1375	1376
300	1820	1.09(14)	1.91(2)	1254	1255
250	1612	8.68(13)	6.54(1)	1055	1056
200	1360	5.25(13)	-2.46(2)	753	754
150	894	1.84(13)	-5.12(2)	362	362

Table 3

Tabular Production rates ($\text{cm}^{-3} \text{ s}^{-1}$) for PIIE flux (full model results in parentheses when different).

ALT	O_2^+	O^+	N_2^+
450	7.28×10^{-3}	1.35×10^1	1.15×10^0
400	3.19×10^{-2}	2.66×10^1	4.11×10^0
350	1.40×10^{-1}	5.02×10^1	1.45×10^1
300	5.01×10^{-1}	7.47×10^1	4.16×10^1
275	7.93×10^{-1}	7.57×10^1	5.93×10^1
250	1.06×10^0	6.32×10^1	7.11×10^1
225	1.11×10^0	4.18×10^1	6.69×10^1
200	8.56×10^{-1}	1.99×10^1	4.63×10^1
180	5.50×10^{-1}	8.49×10^0 (8.50×10^0)	2.78×10^1
160	5.91×10^{-1} (5.92×10^{-1})	6.01×10^0 (6.00×10^0)	2.69×10^1
145	6.20×10^{-1}	4.44×10^0 (4.45×10^0)	2.54×10^1
130	3.32×10^{-1}	1.58×10^0	1.19×10^1
120	3.64×10^{-2}	1.22×10^{-1}	1.15×10^0
115	1.07×10^{-3}	2.78×10^{-3}	2.98×10^{-2} (2.99×10^{-2})
ALT	$\text{O}_2(1\text{DELG})$	$\text{O}(1\text{D})$	$\text{N}_2(\text{A3})$
450	1.81×10^{-3} (1.69×10^{-3})	1.19×10^1 (1.12×10^1)	4.04×10^{-1} (3.87×10^{-1})
400	1.14×10^{-2} (1.09×10^{-2})	3.34×10^1 (3.20×10^1)	1.74×10^0 (1.68×10^0)
350	7.55×10^{-2} (7.35×10^{-2})	9.42×10^1 (9.18×10^1)	7.70×10^0 (7.50×10^0)
300	4.37×10^{-1} (4.31×10^{-1})	2.27×10^2 (2.24×10^2)	2.95×10^1 (2.91×10^1)
275	8.95×10^{-1} (8.87×10^{-1})	3.01×10^2 (2.98×10^2)	4.84×10^1 (4.78×10^1)
250	1.52×10^0 (1.51×10^0)	3.25×10^2 (3.23×10^2)	6.37×10^1 (6.33×10^1)
225	1.93×10^0	2.63×10^2	6.03×10^1 (6.02×10^1)
200	1.65×10^0	1.38×10^2	3.78×10^1
180	1.06×10^0	5.83×10^1	1.83×10^1
160	1.24×10^0	4.34×10^1	1.63×10^1
145	1.45×10^0	3.24×10^1	1.58×10^1
130	9.03×10^{-1}	1.29×10^1	7.66×10^0
120	1.14×10^{-1}	1.02×10^0	7.70×10^{-1}
115	3.70×10^{-3} (3.69×10^{-3})	2.28×10^{-2} (2.29×10^{-2})	2.07×10^{-2}

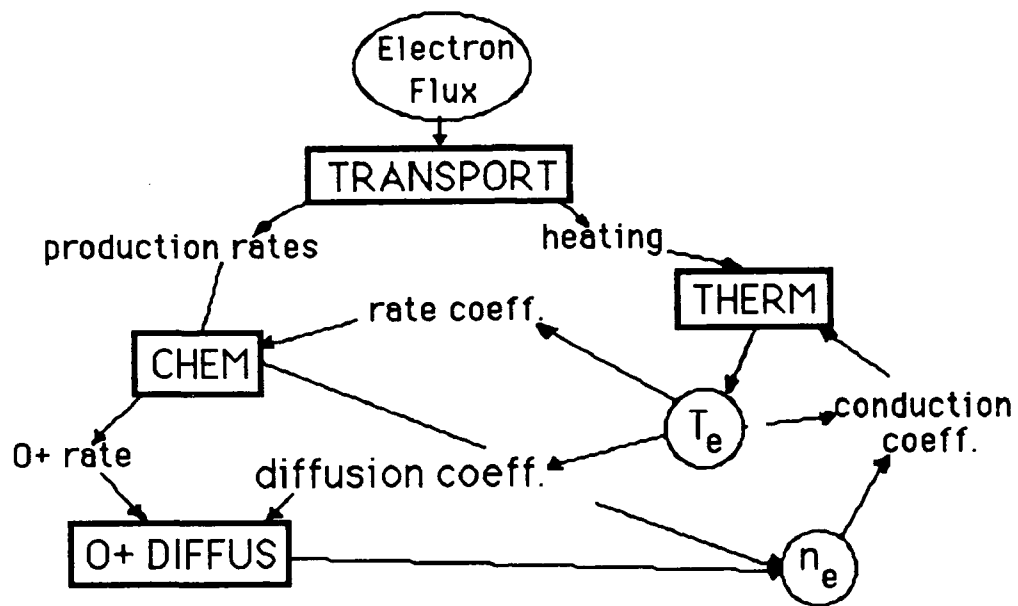


Figure 1

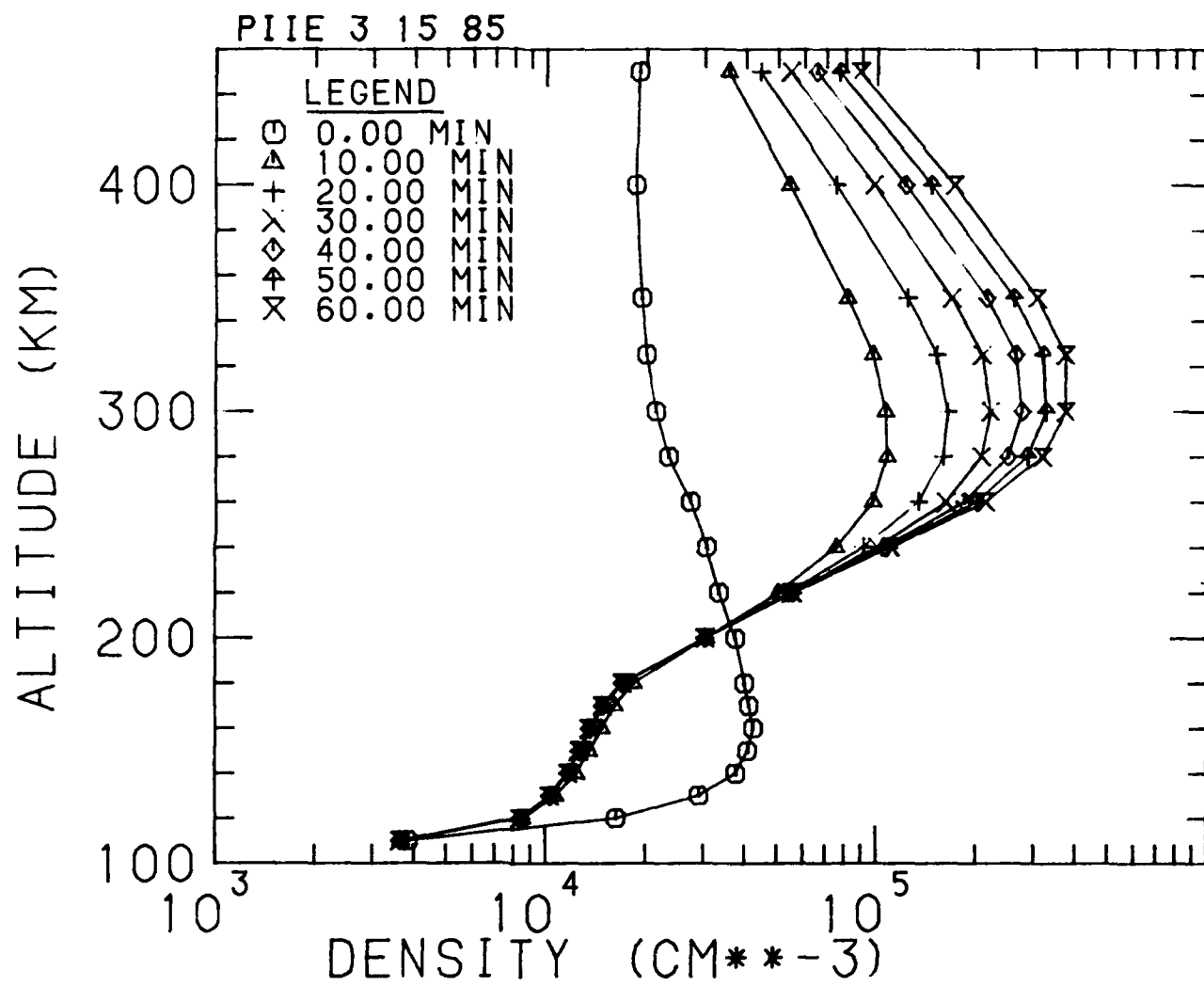


Figure 2
53

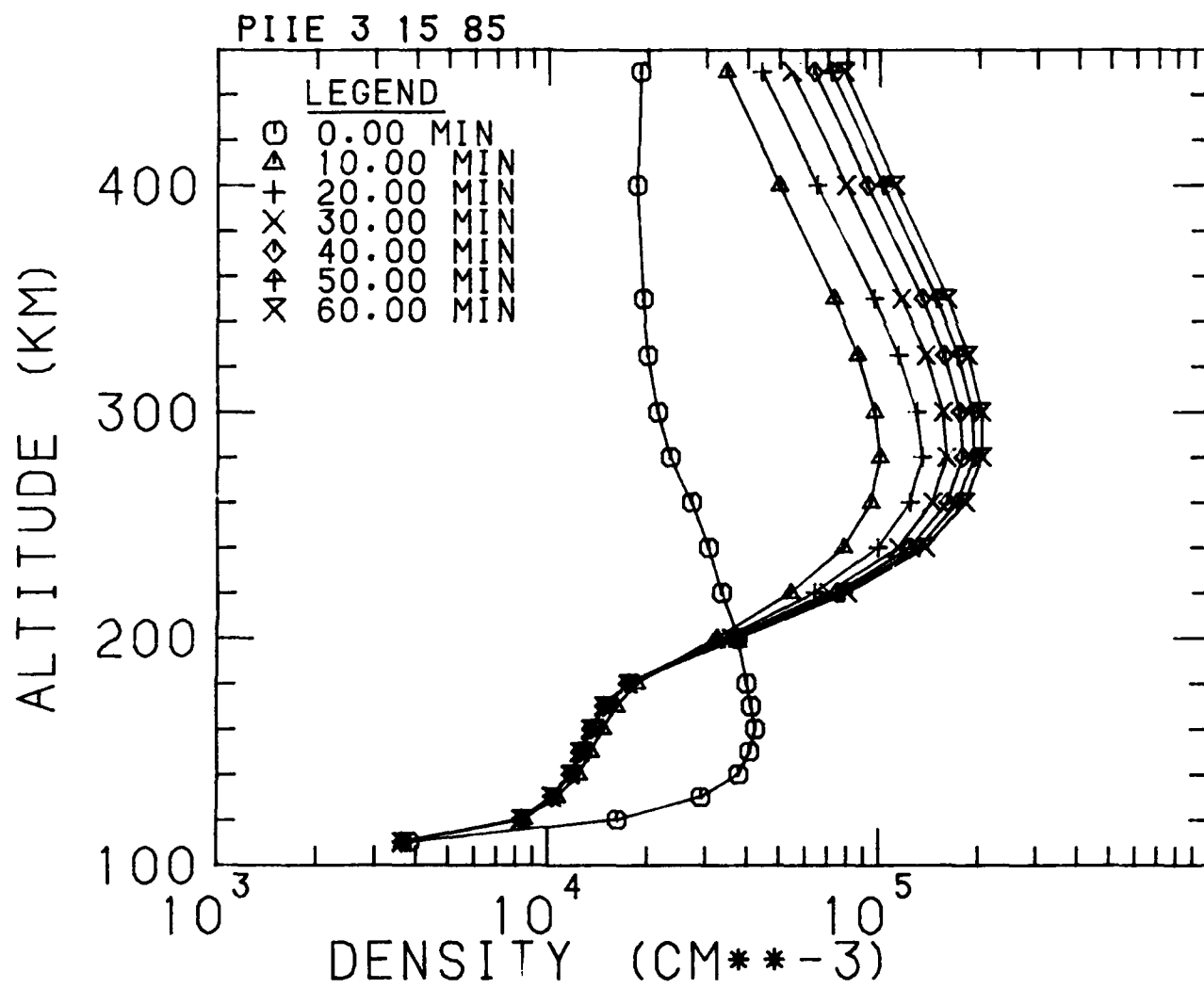


Figure 3

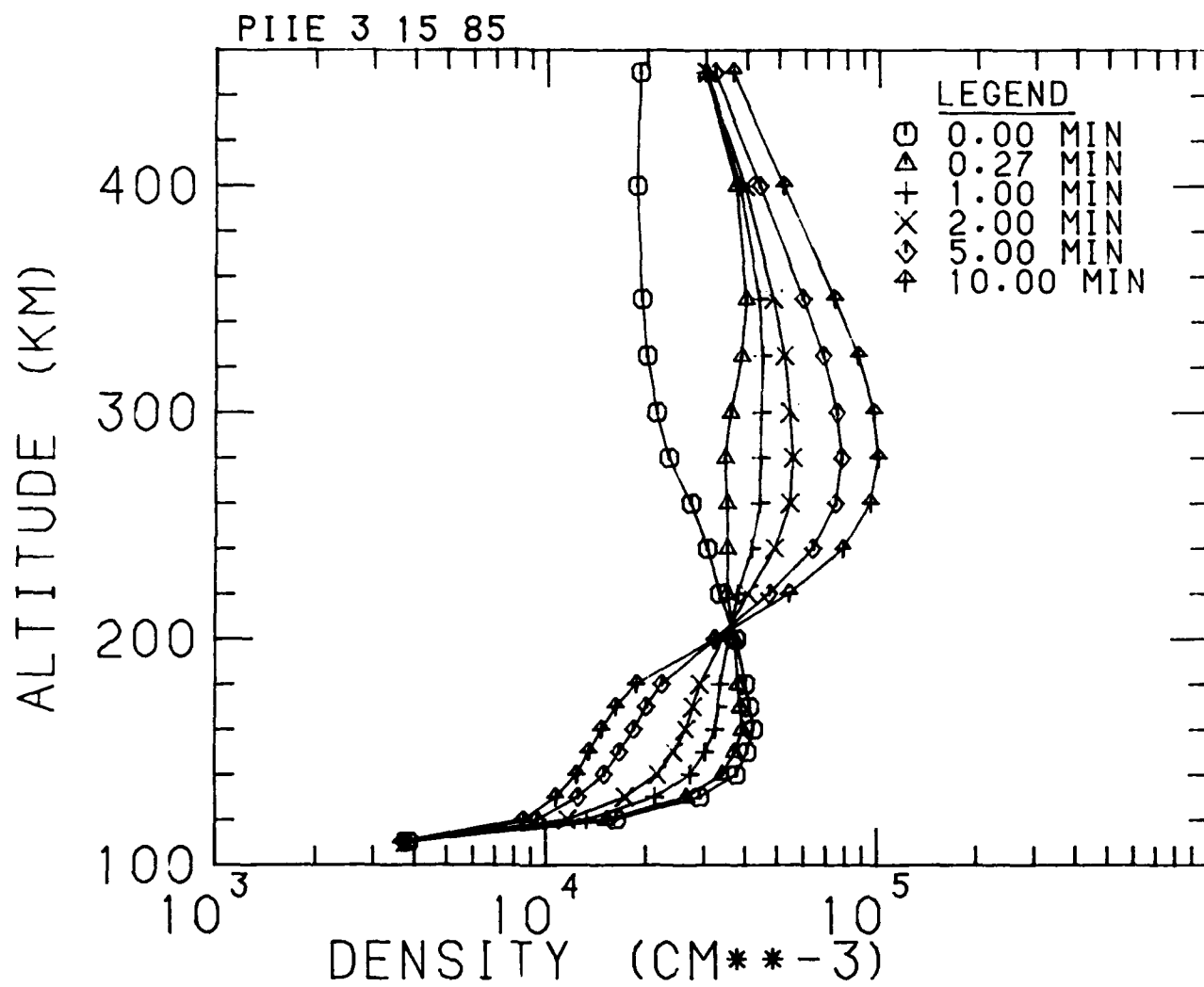


Figure 4a

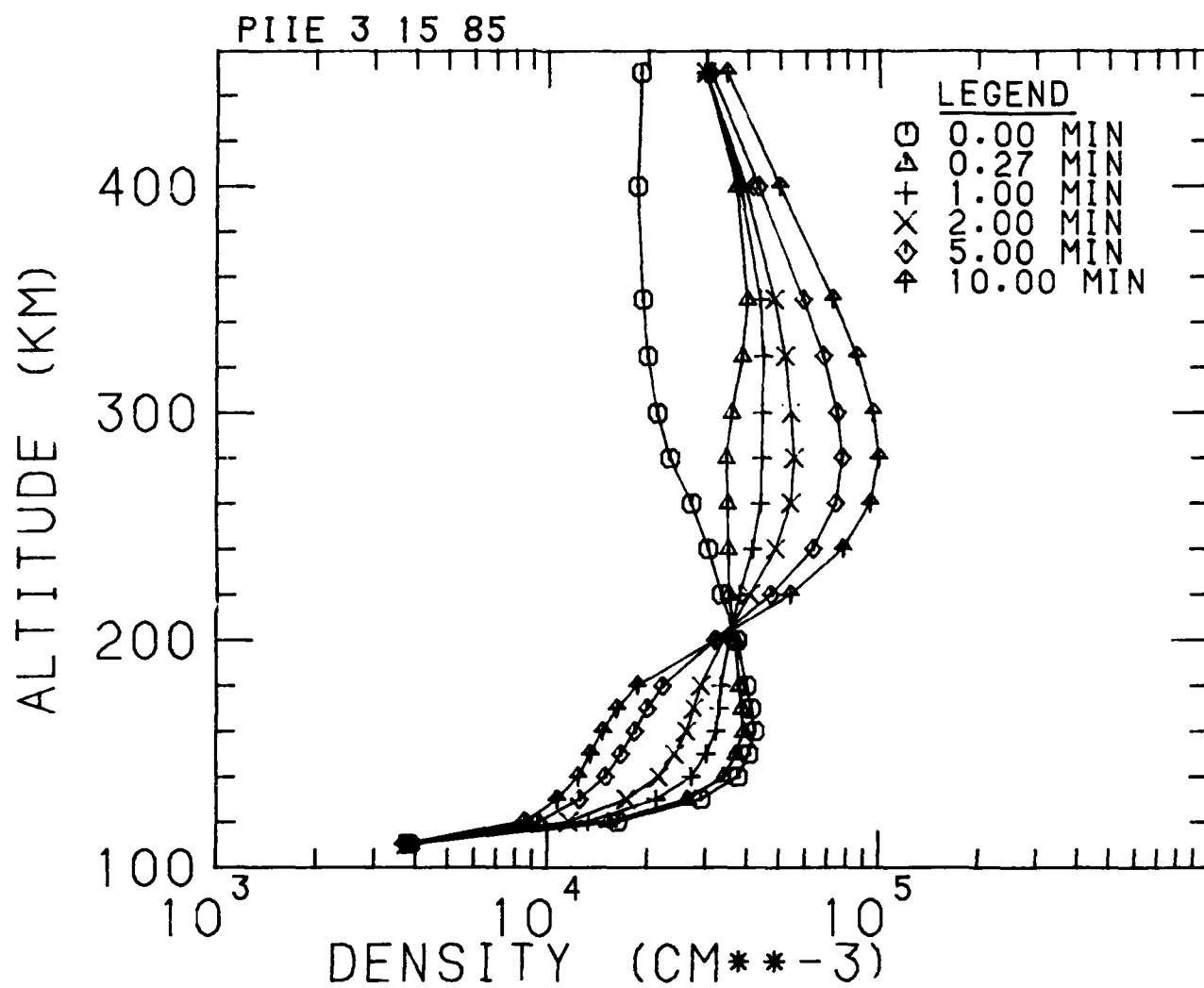


Figure 4b

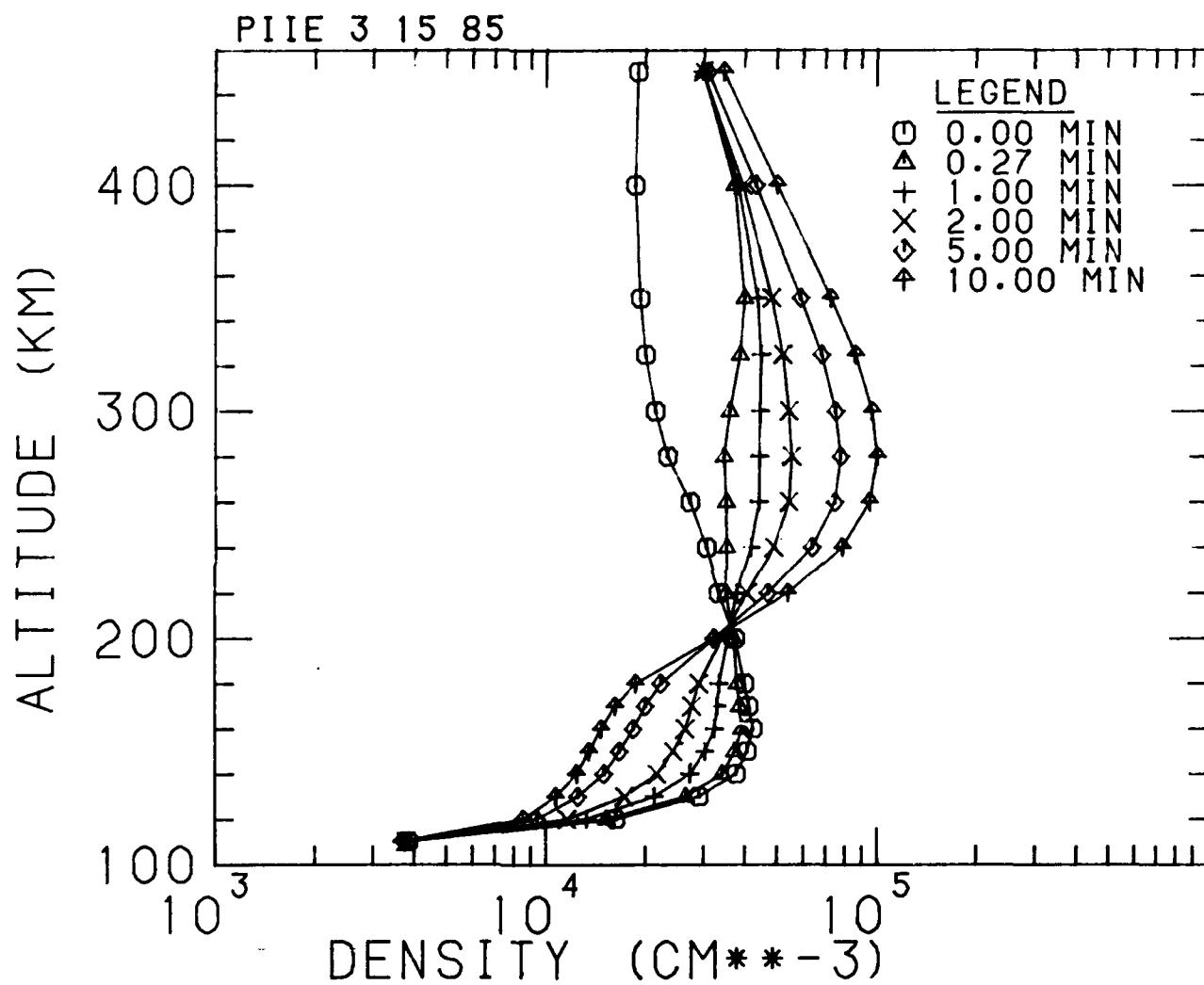


Figure 4c

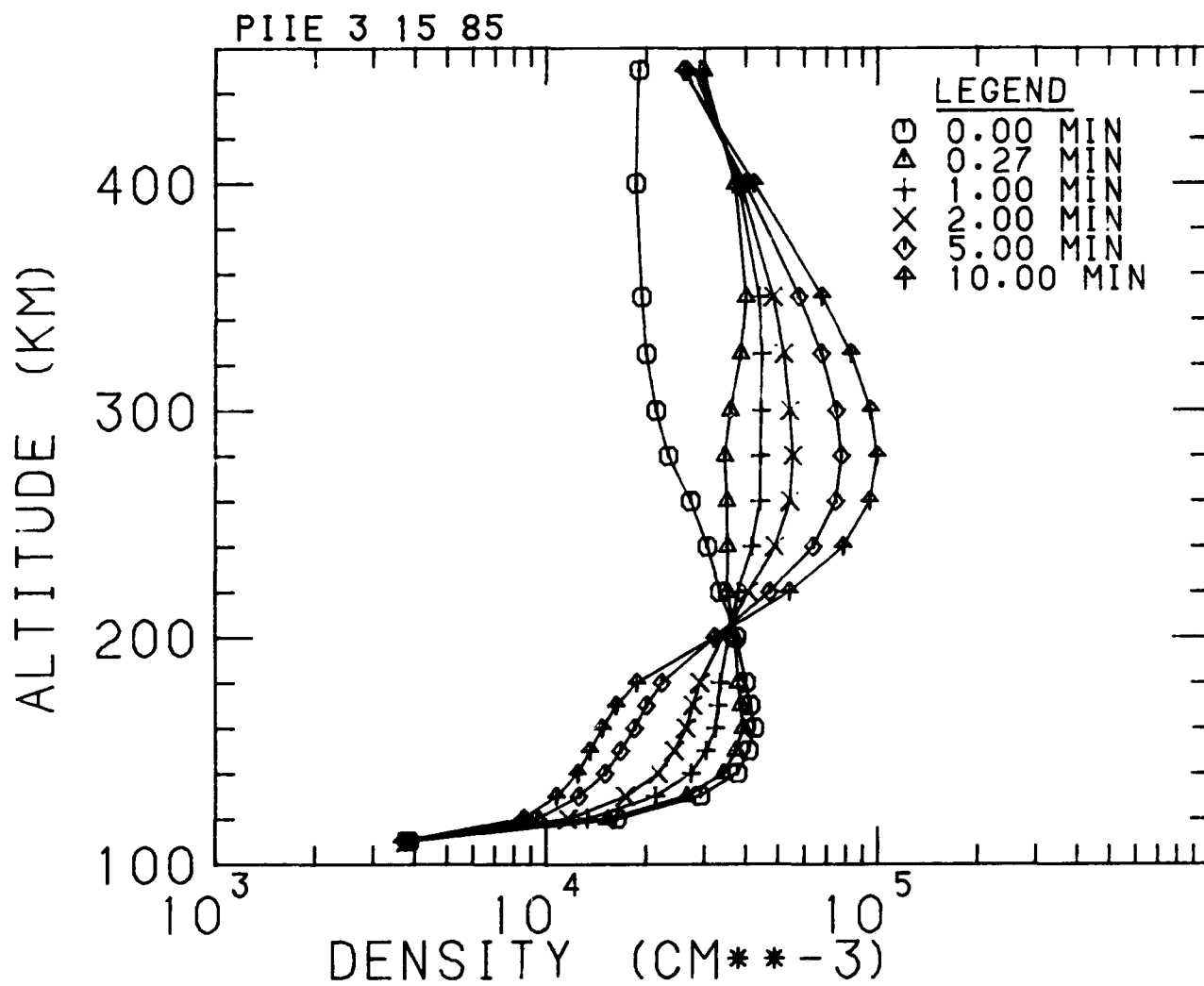
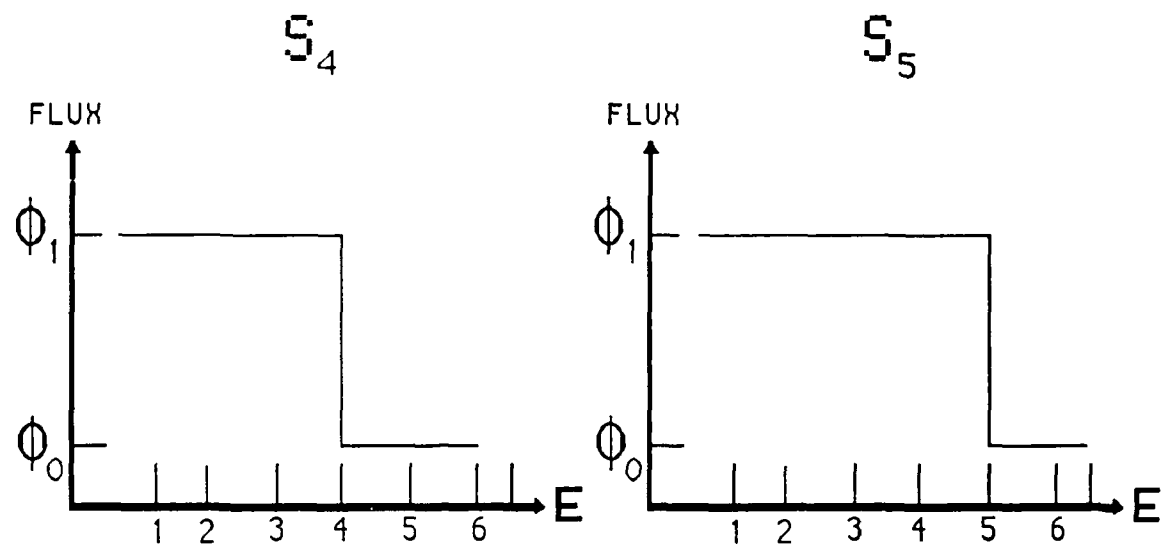


Figure 4d



$$\begin{aligned}
 P_{4-5} &= \text{PRODUCTION FROM } E_4 \text{ TO } E_5 \\
 &= P(S_5) - P(S_4)
 \end{aligned}$$

Figure 5

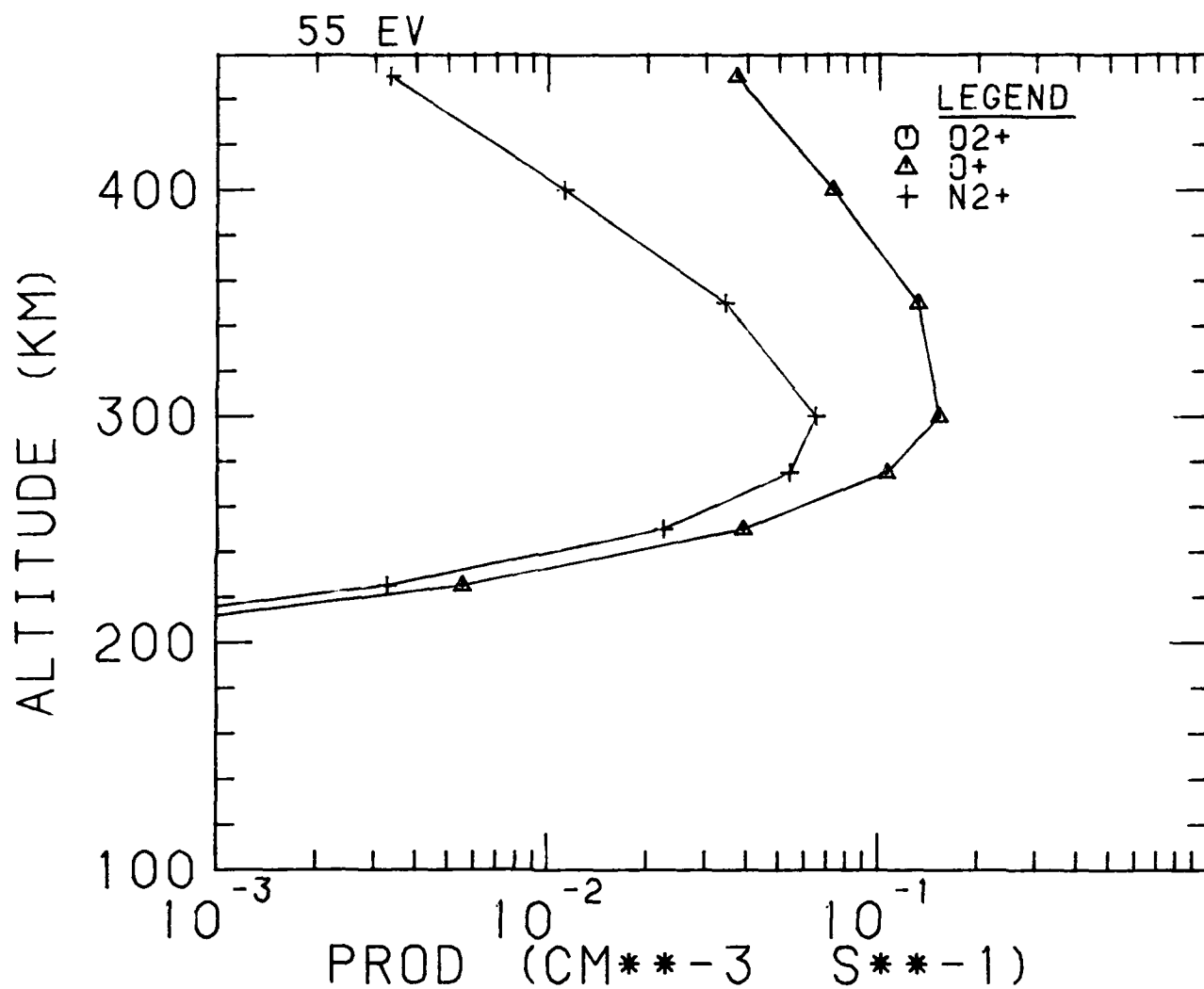


Figure 6a

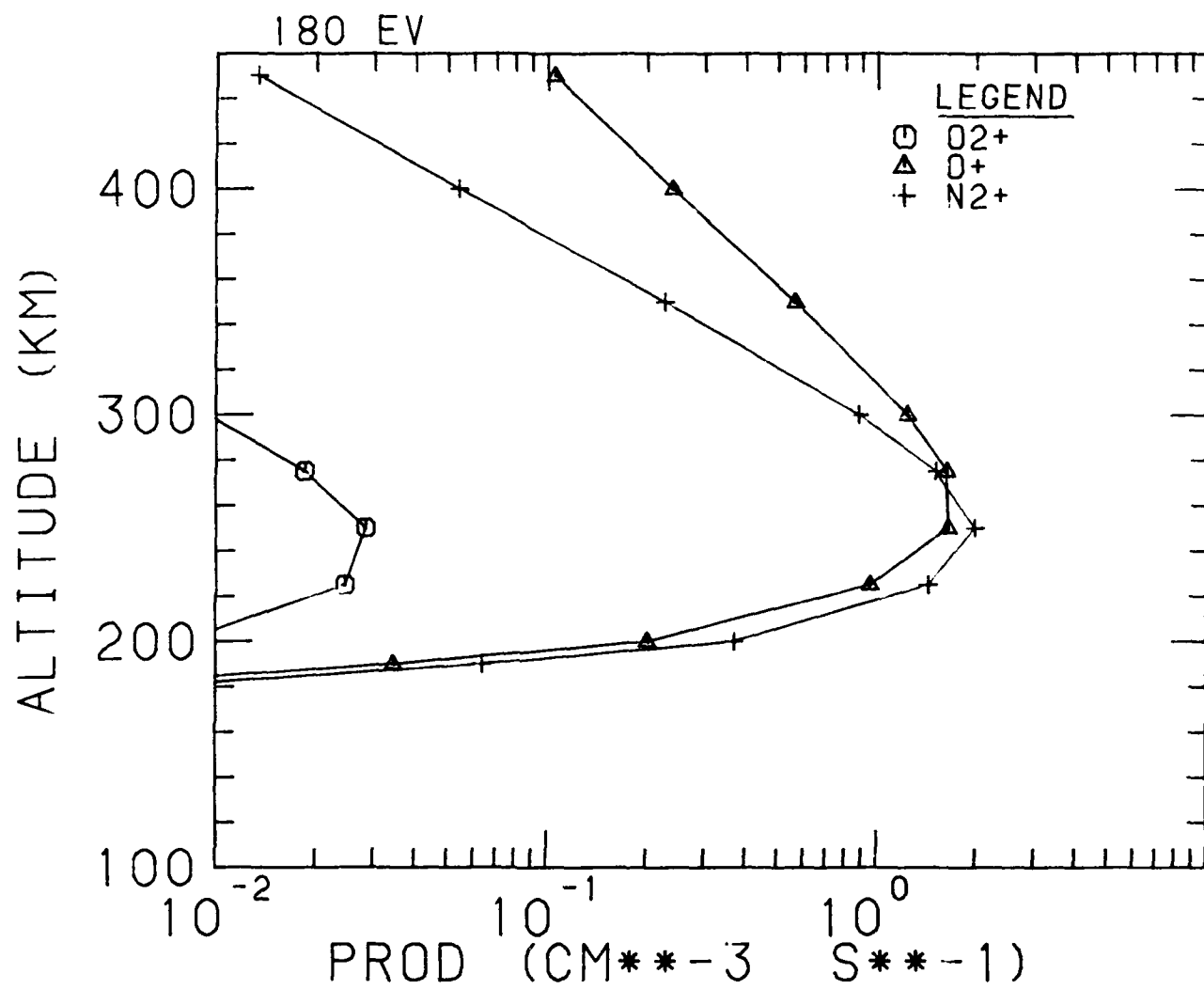
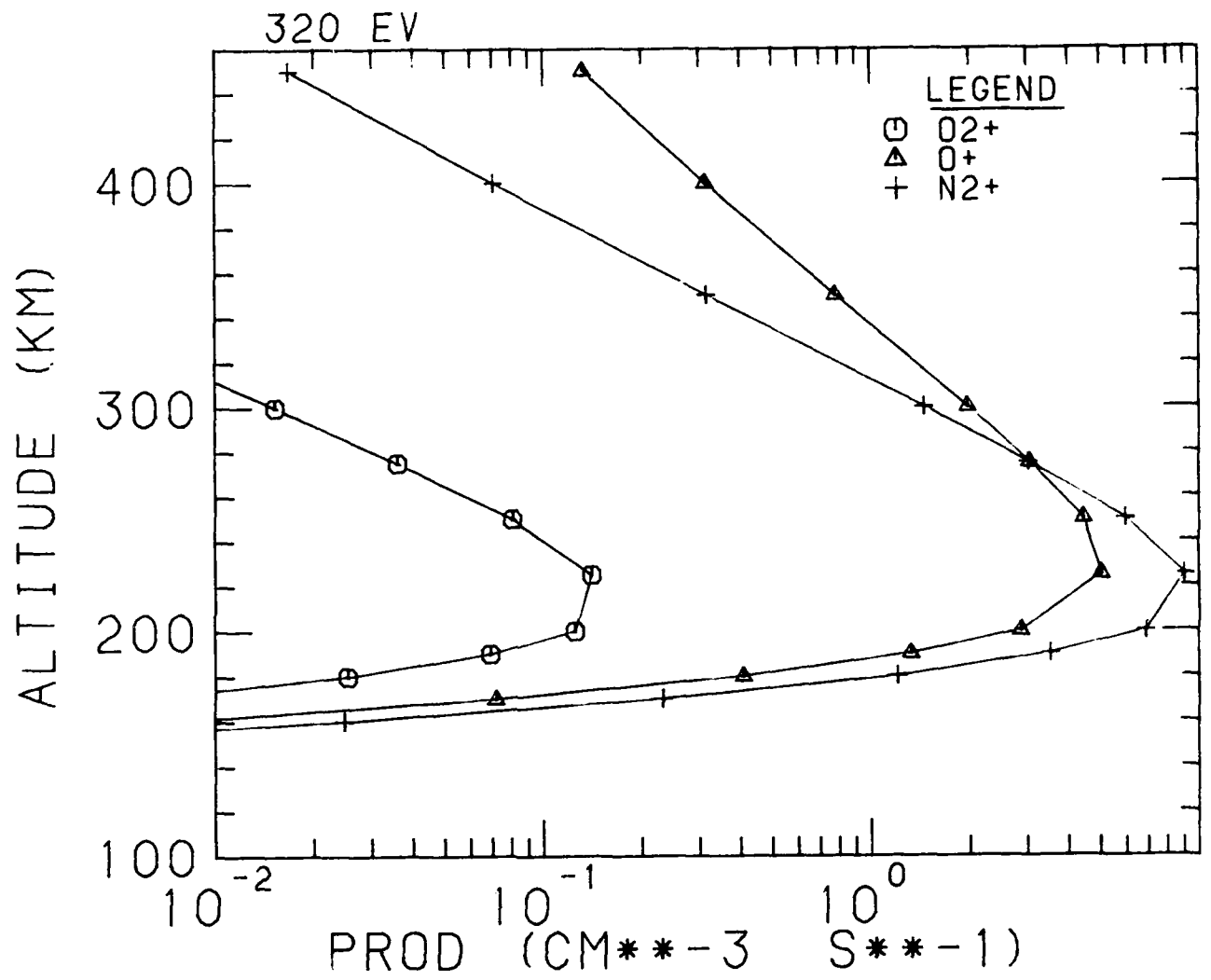


Figure 6b
61



Figur 6c

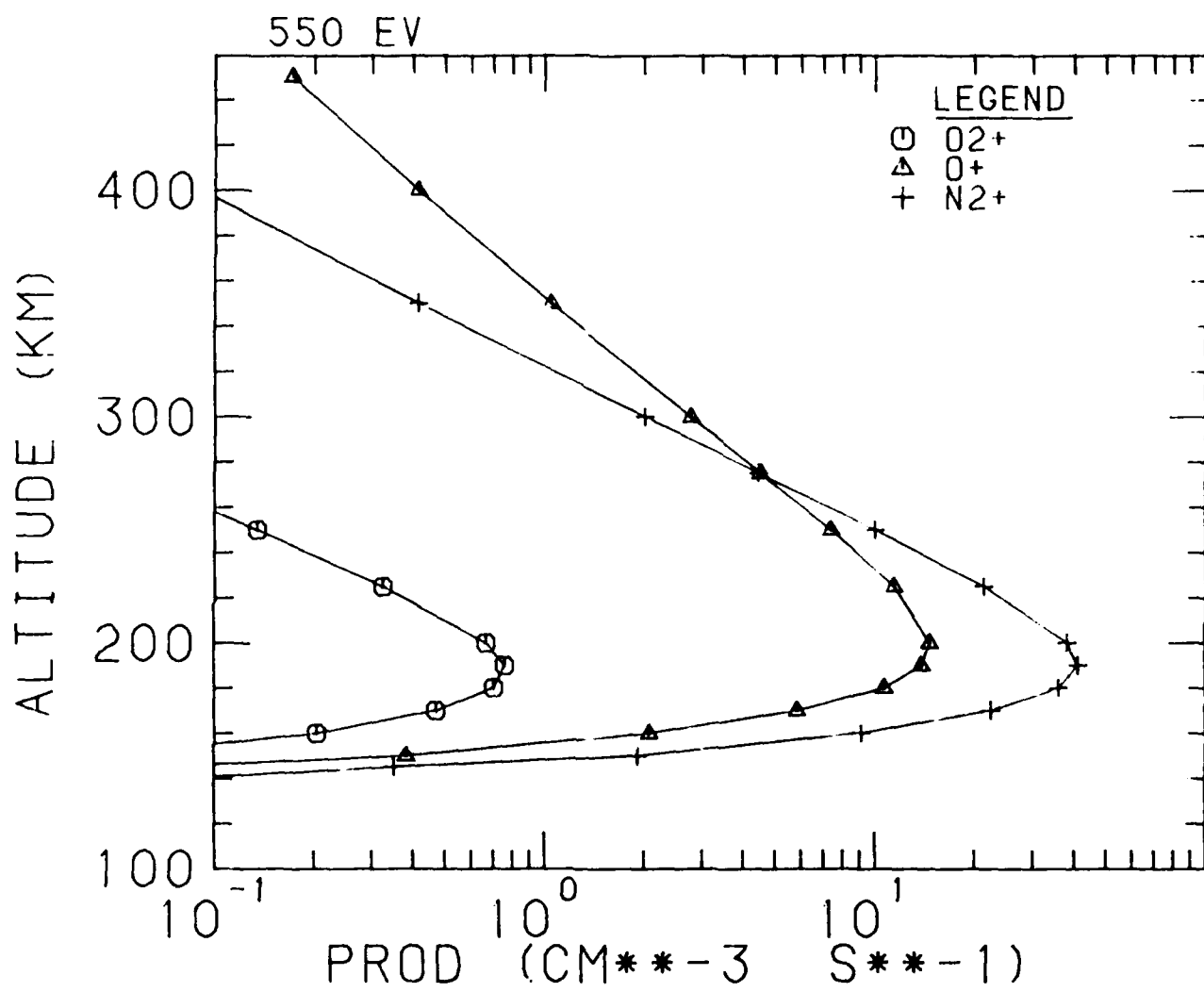


Figure 6d

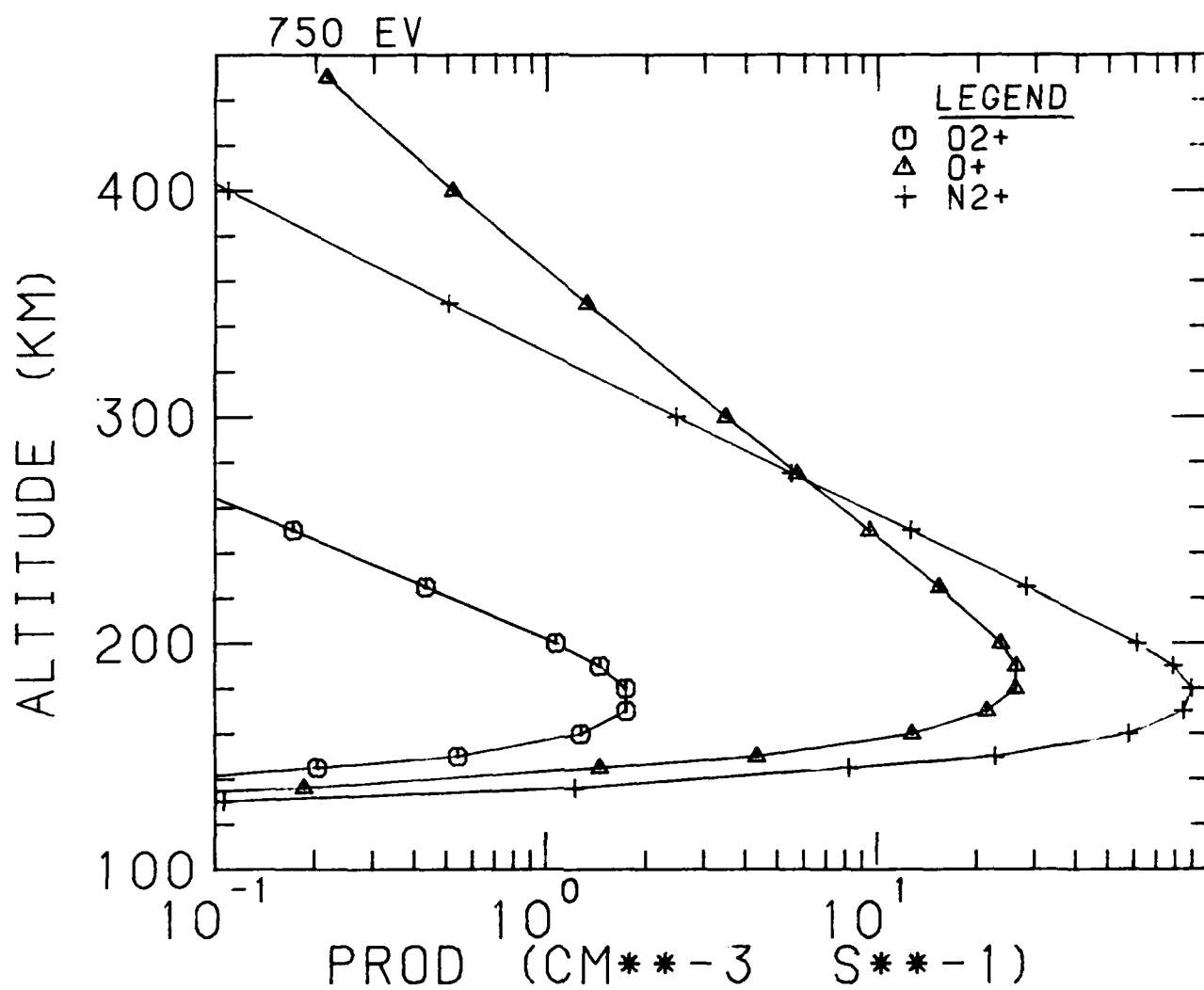


Figure 6e

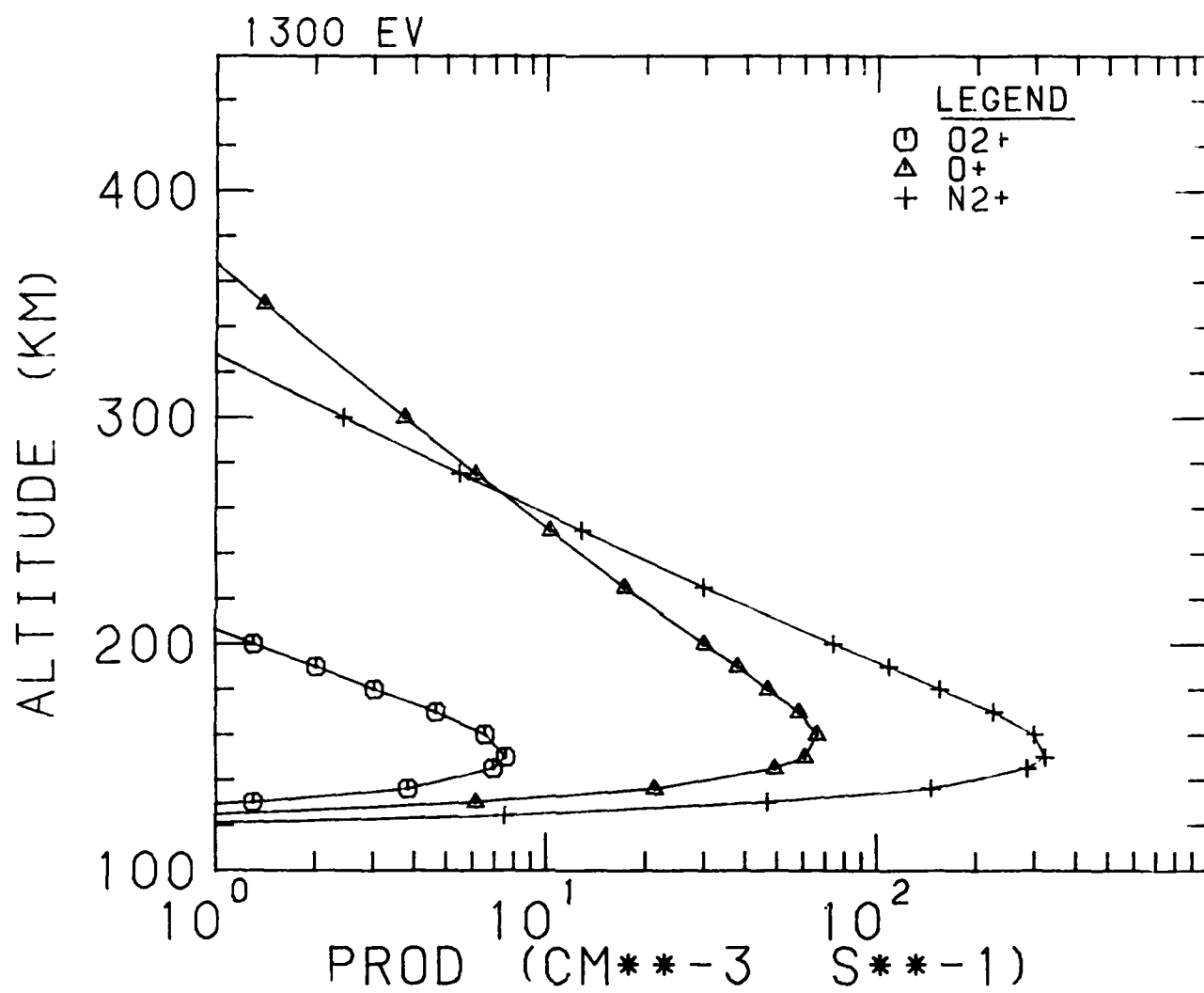


Figure 6f

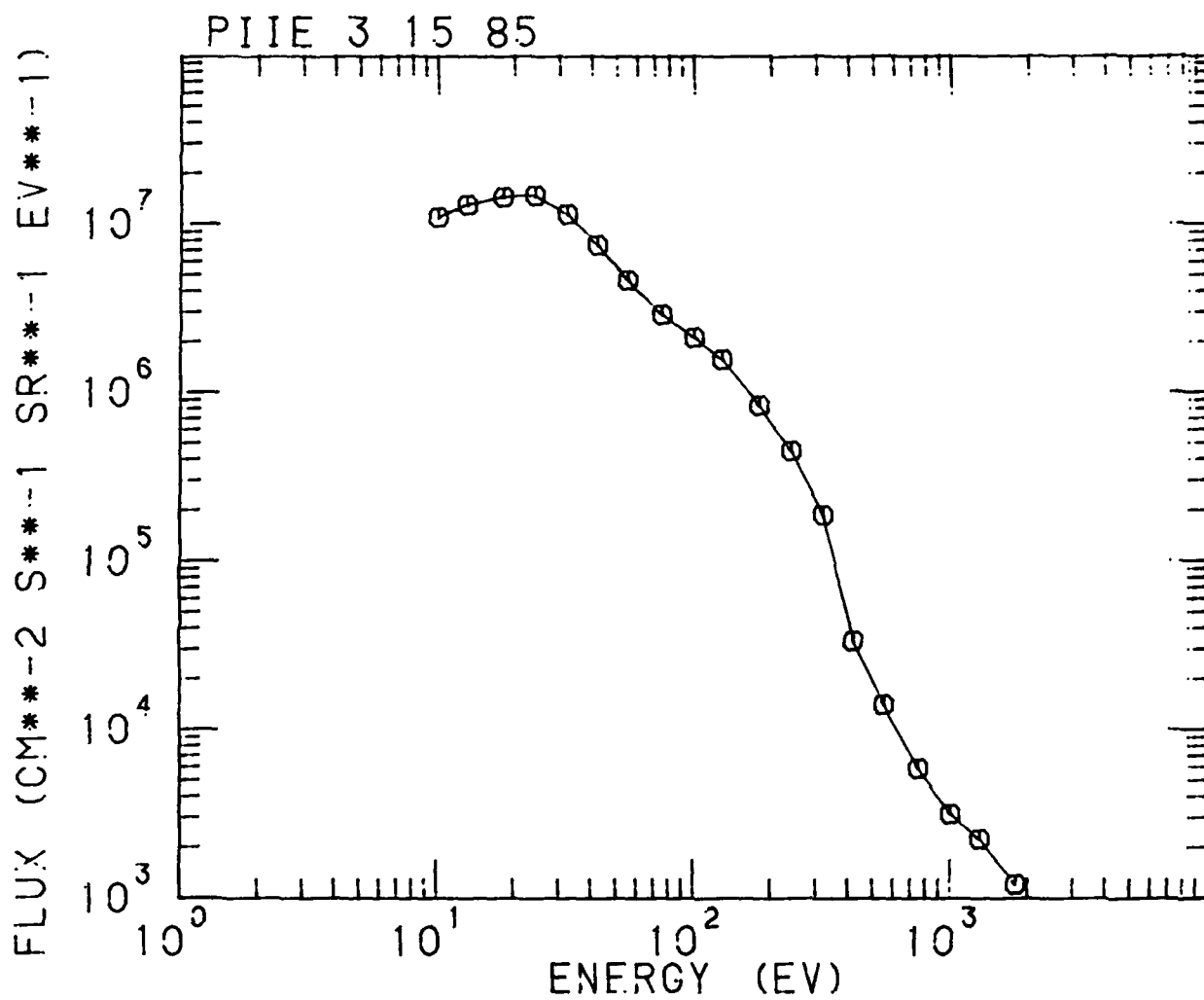


Figure 7a

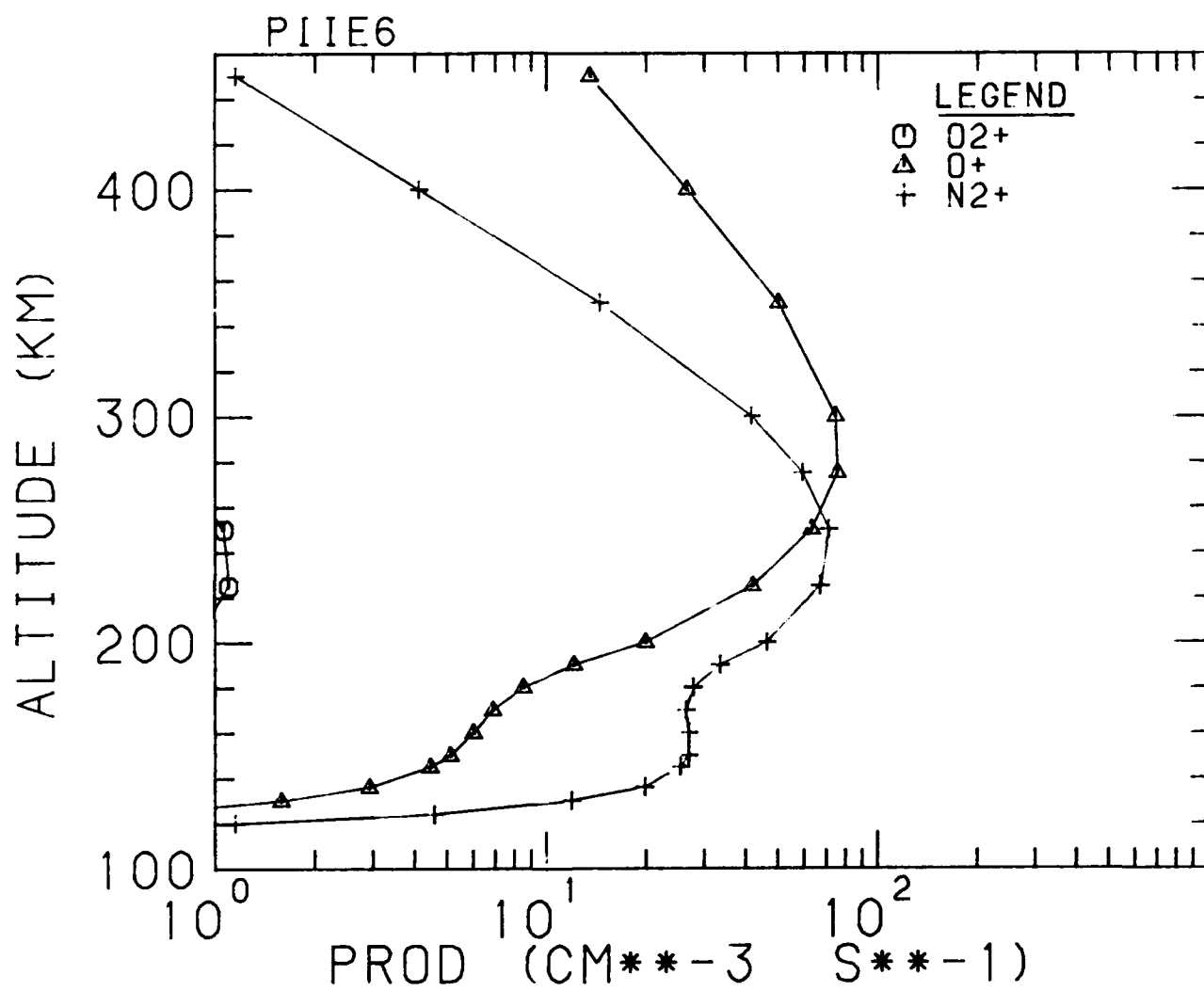


Figure 7b

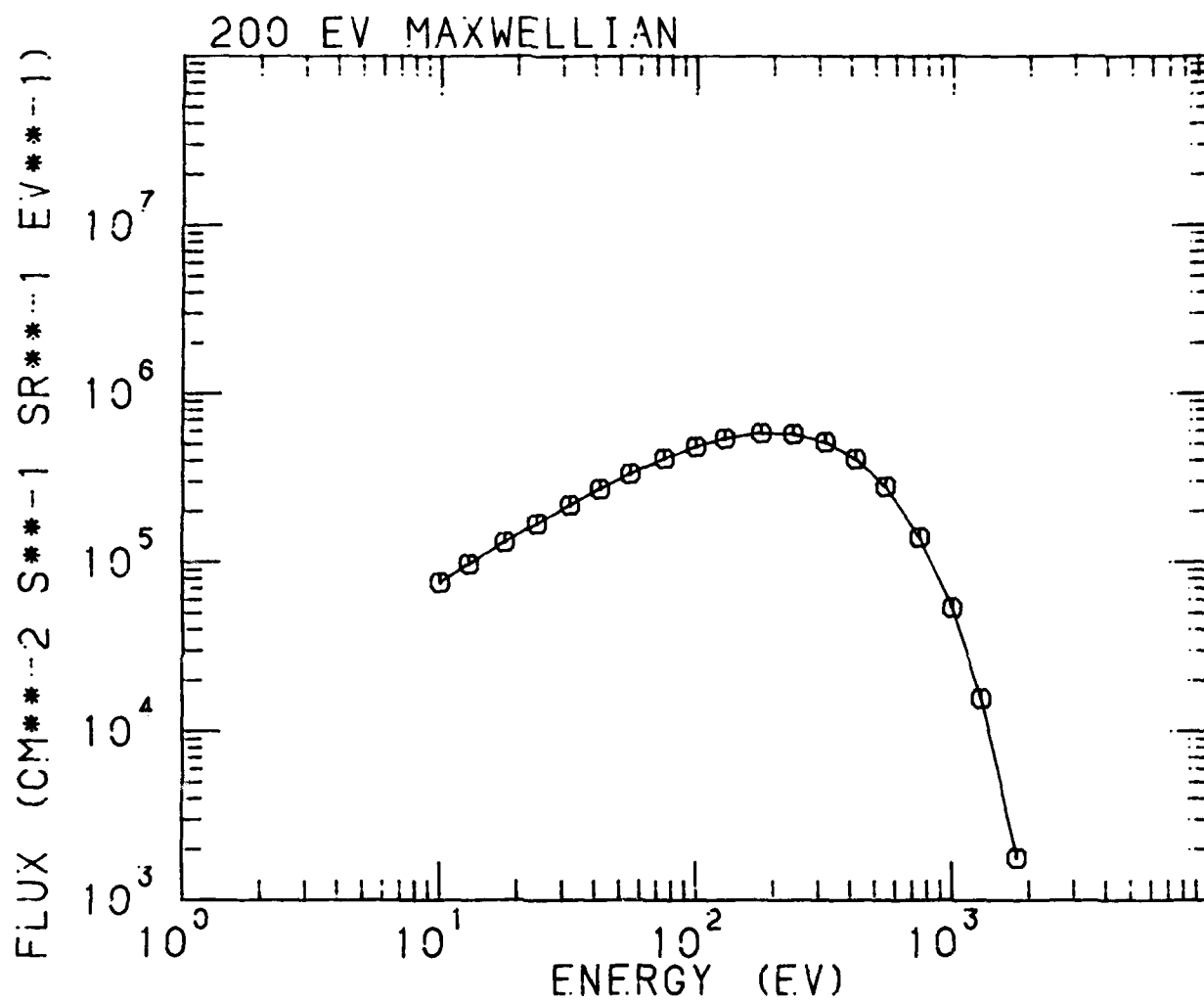


Figure 8a

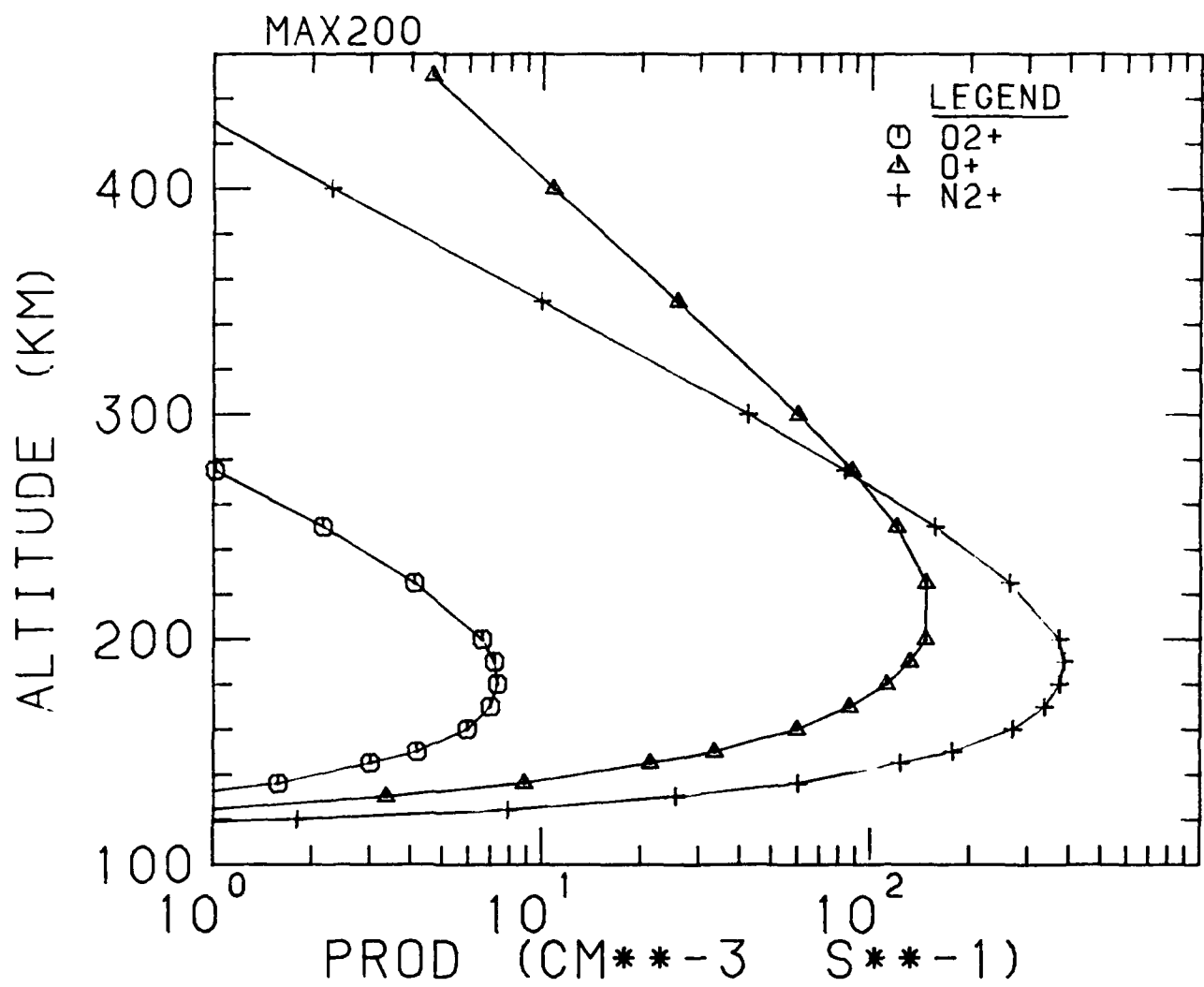


Figure 8b

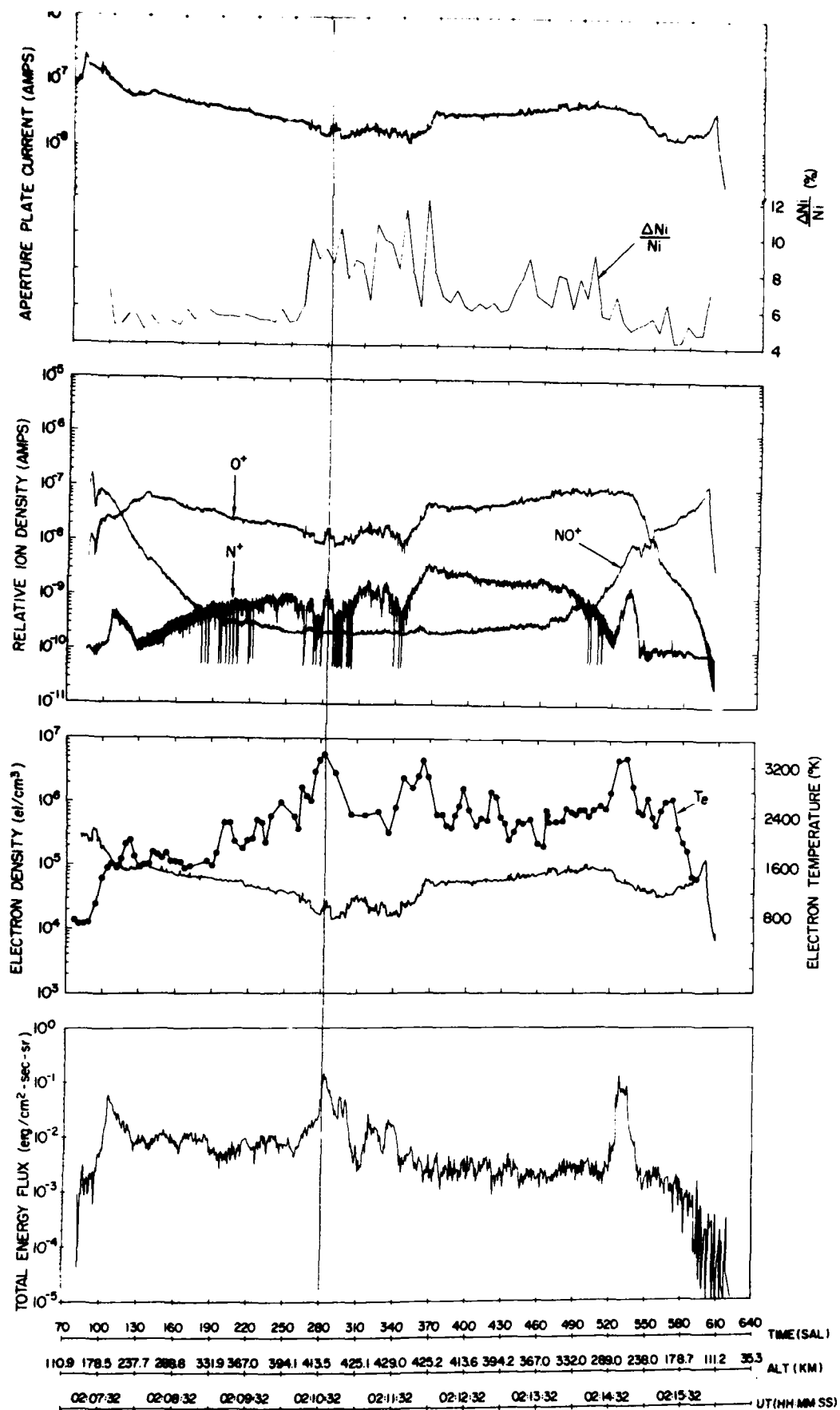


Figure 9

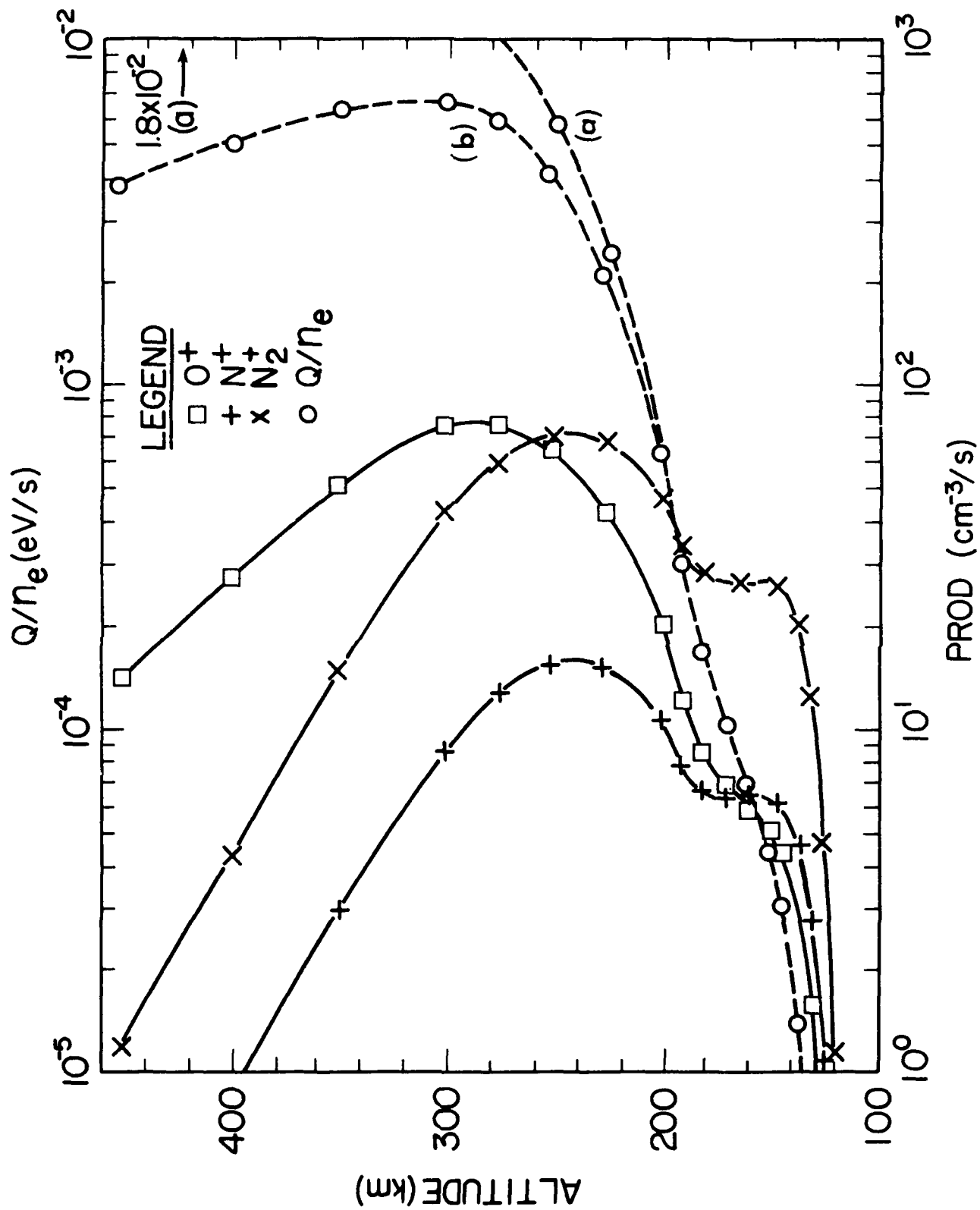


Figure 10

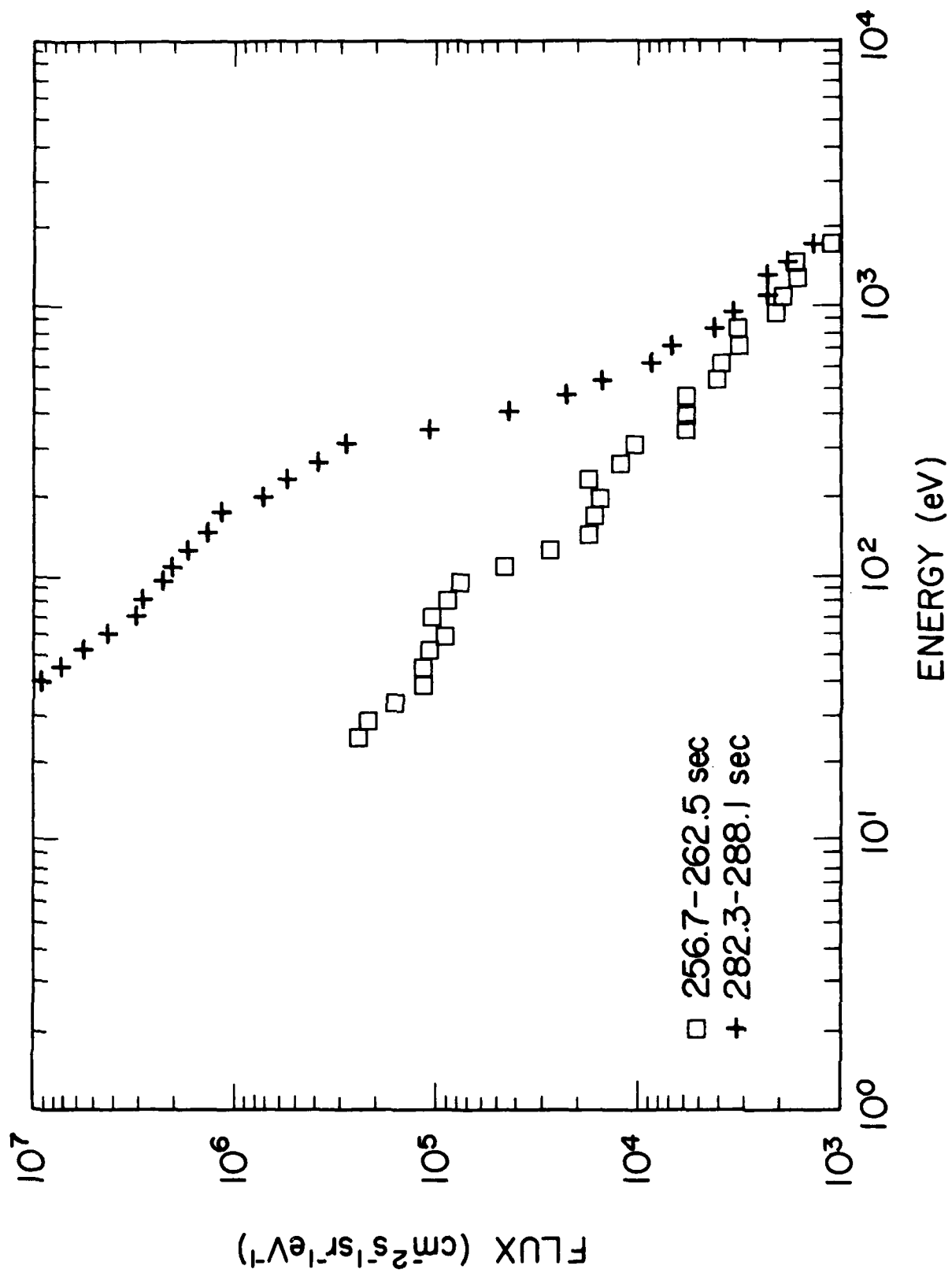


Figure 11

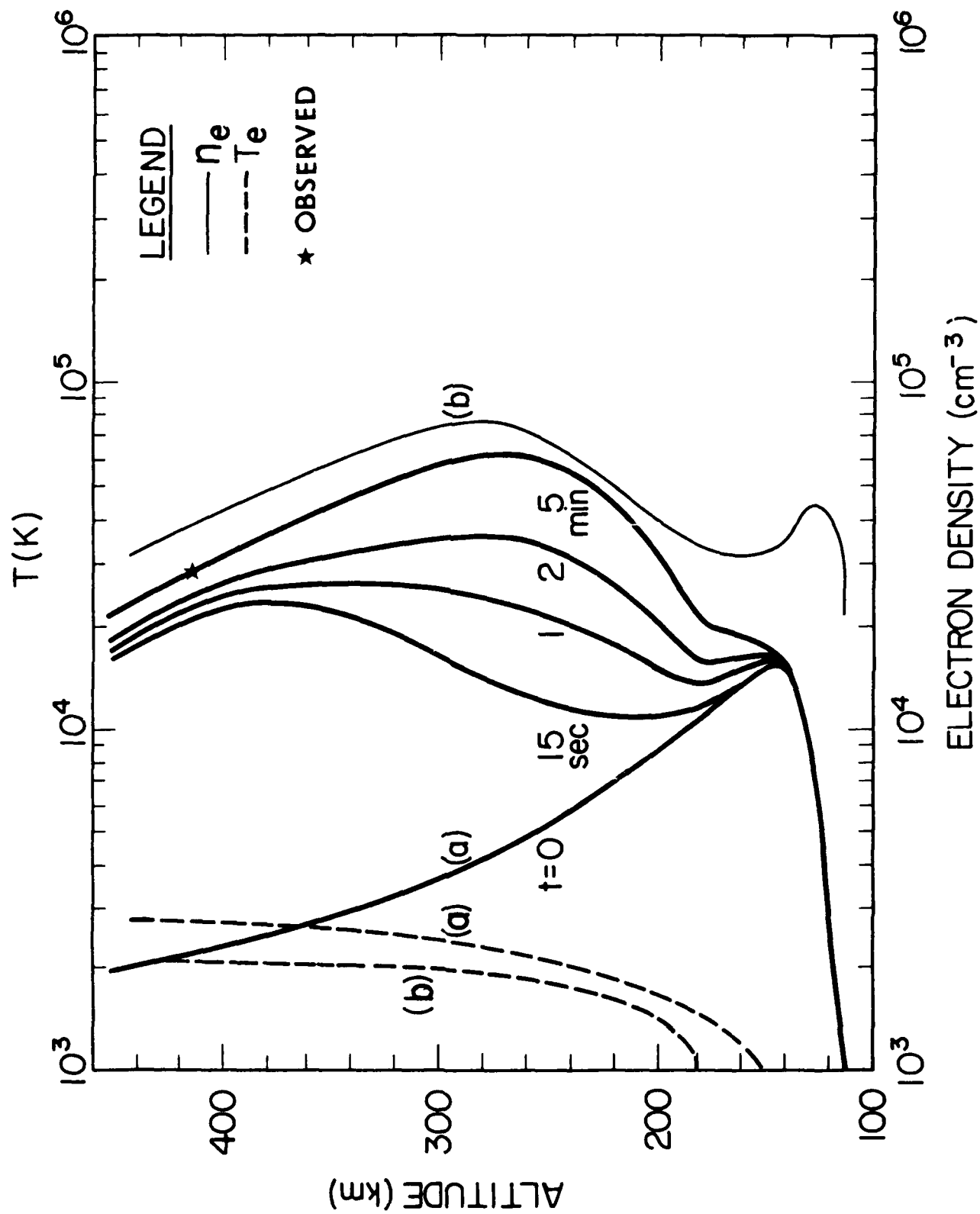


Figure 12

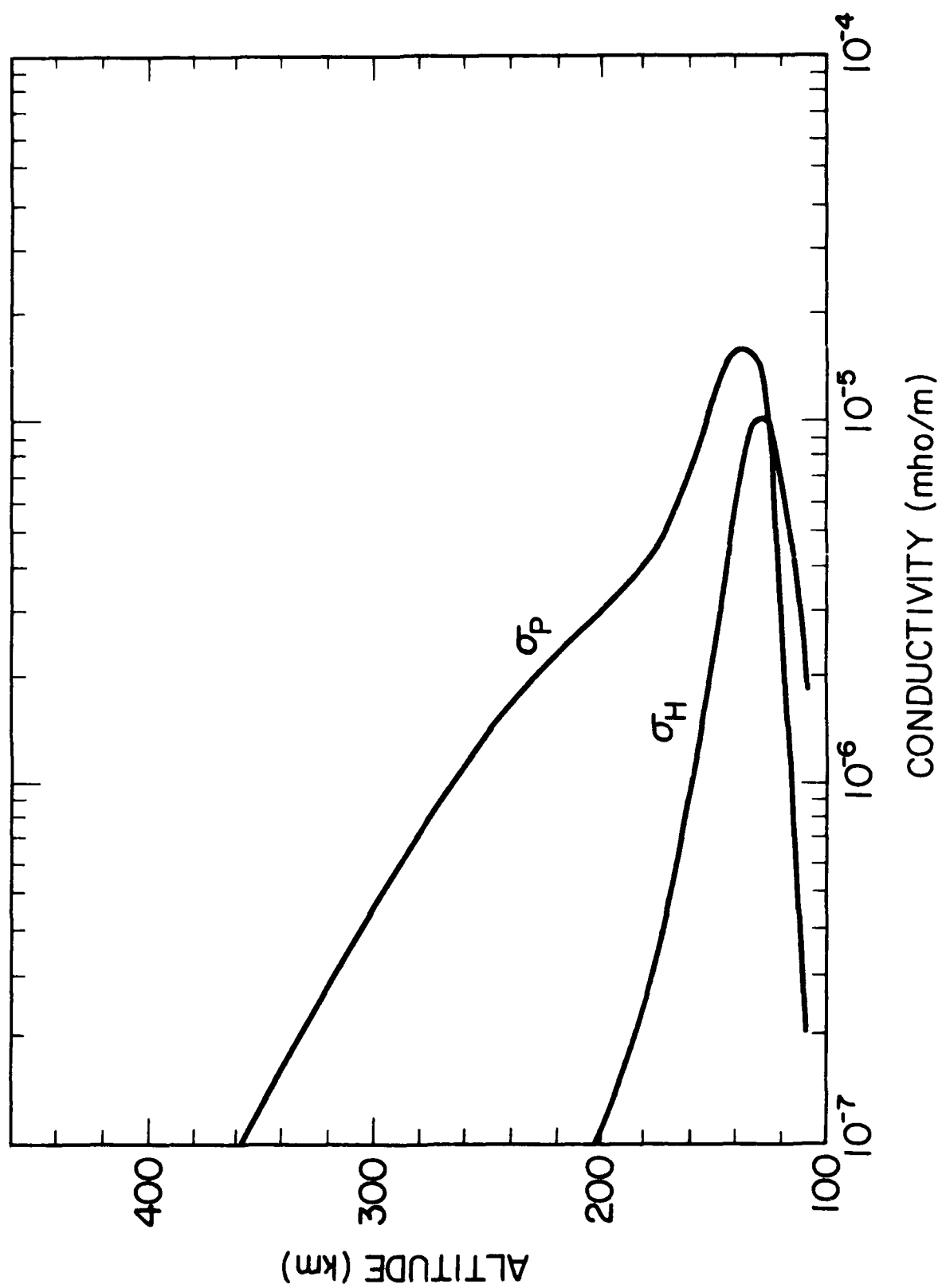


Figure 13

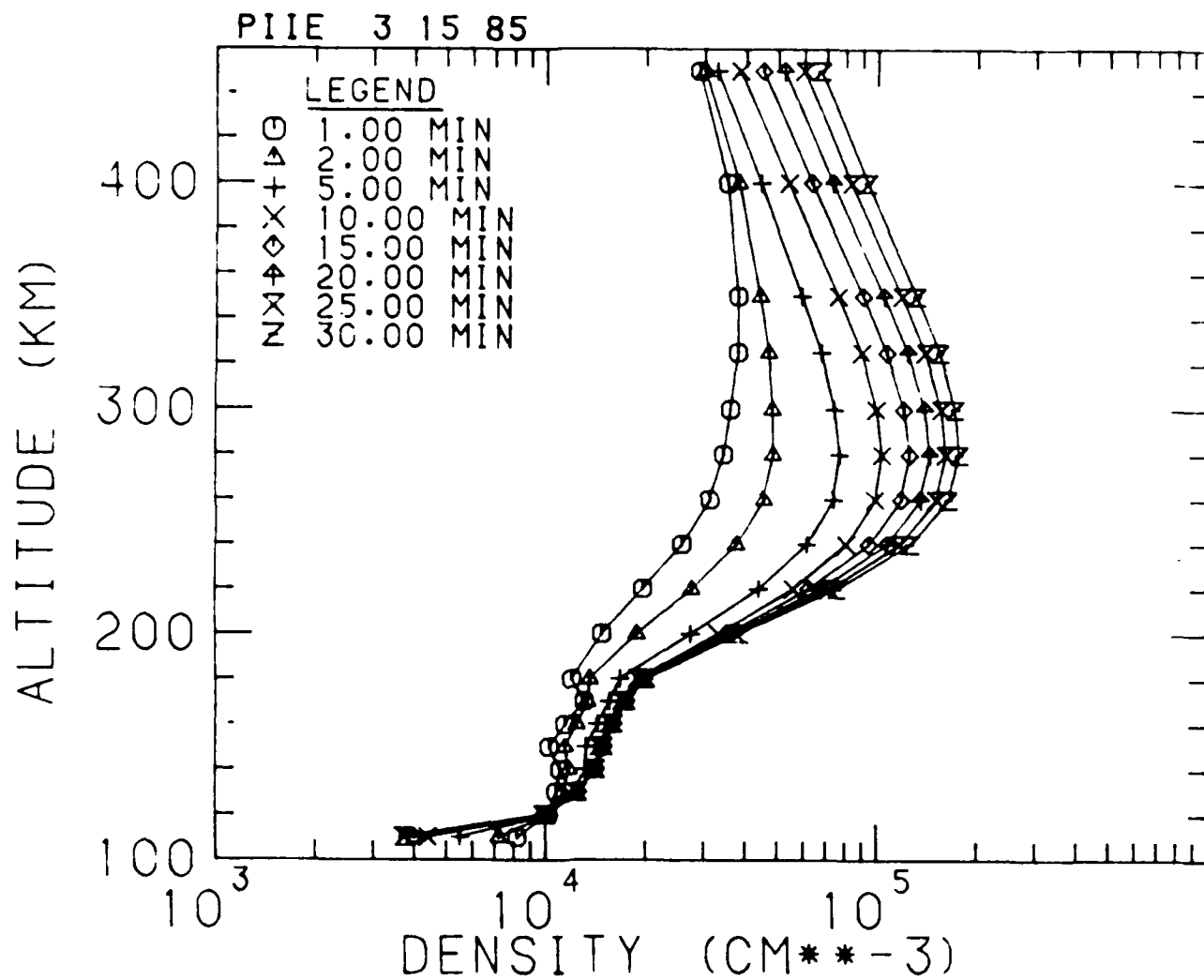


Figure 14

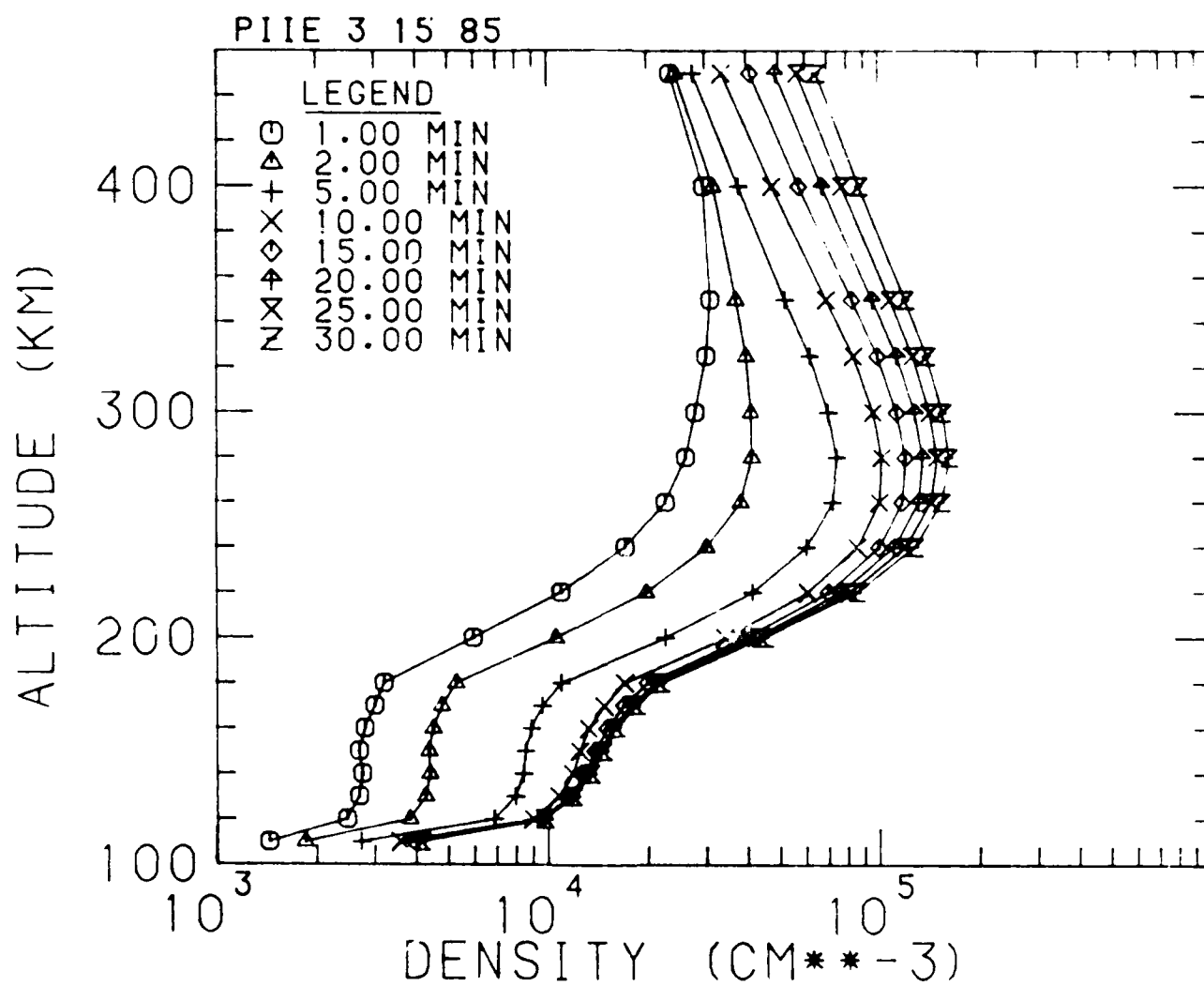


Figure 15

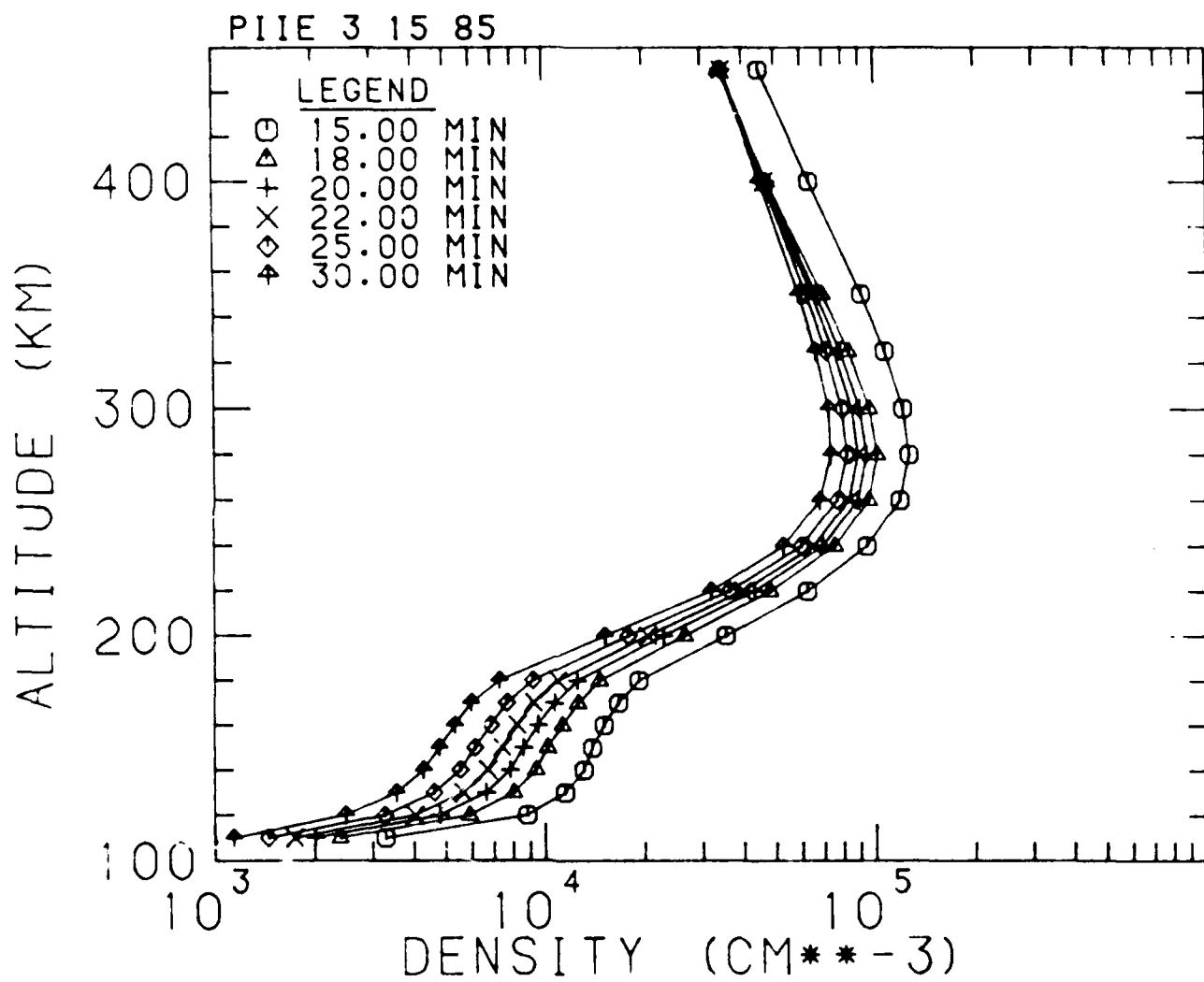


Figure 16

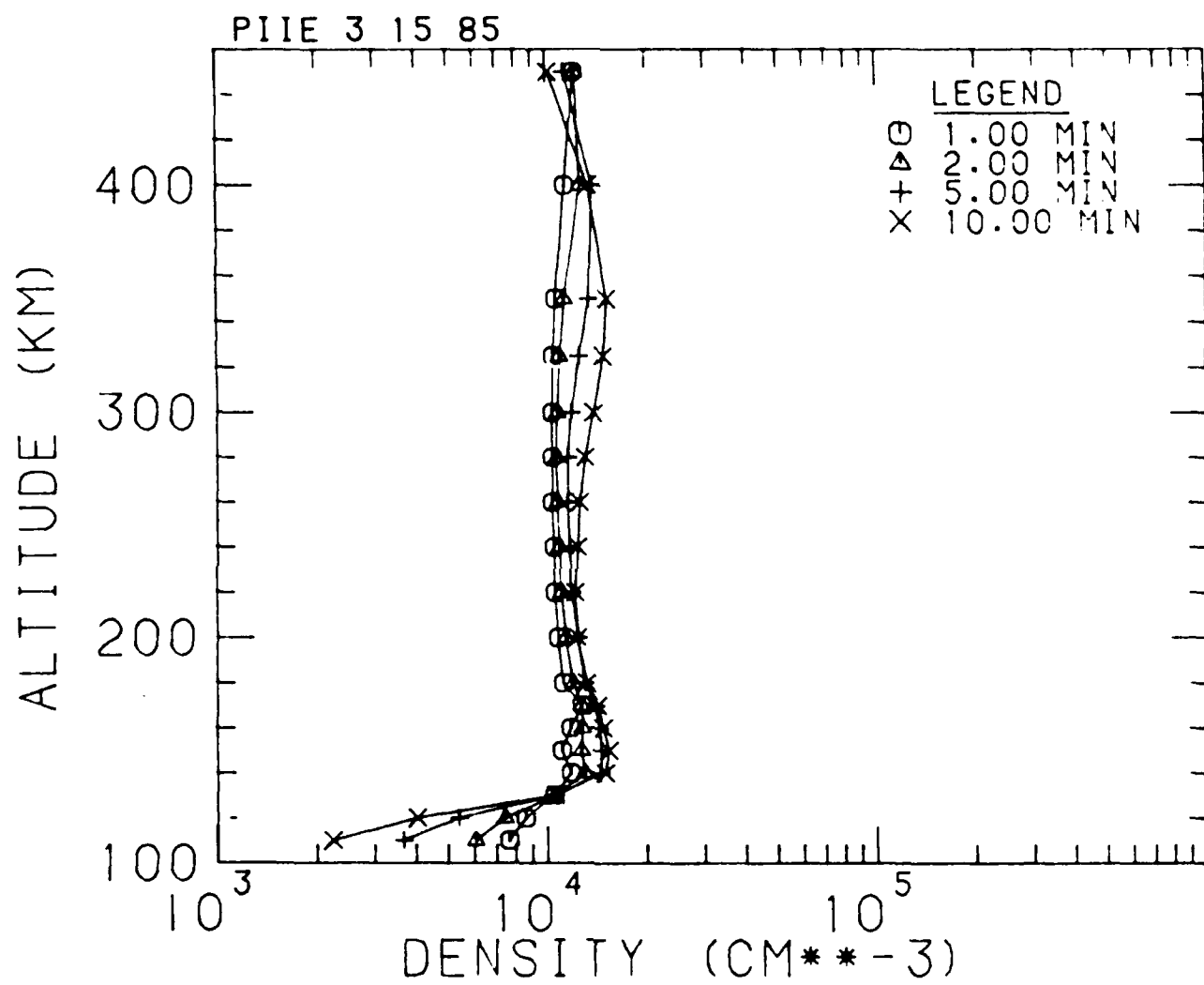


Figure 17

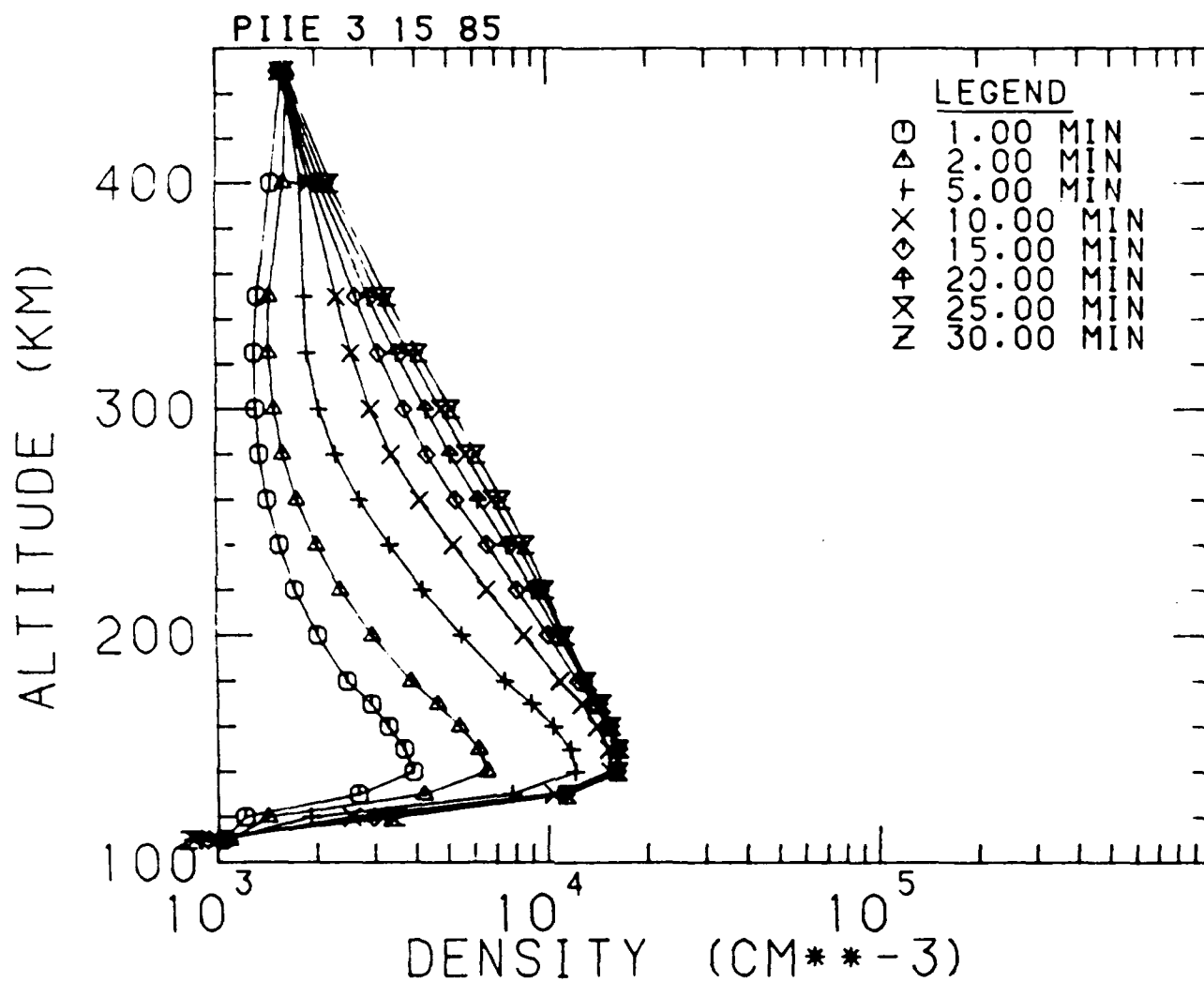


Figure 18

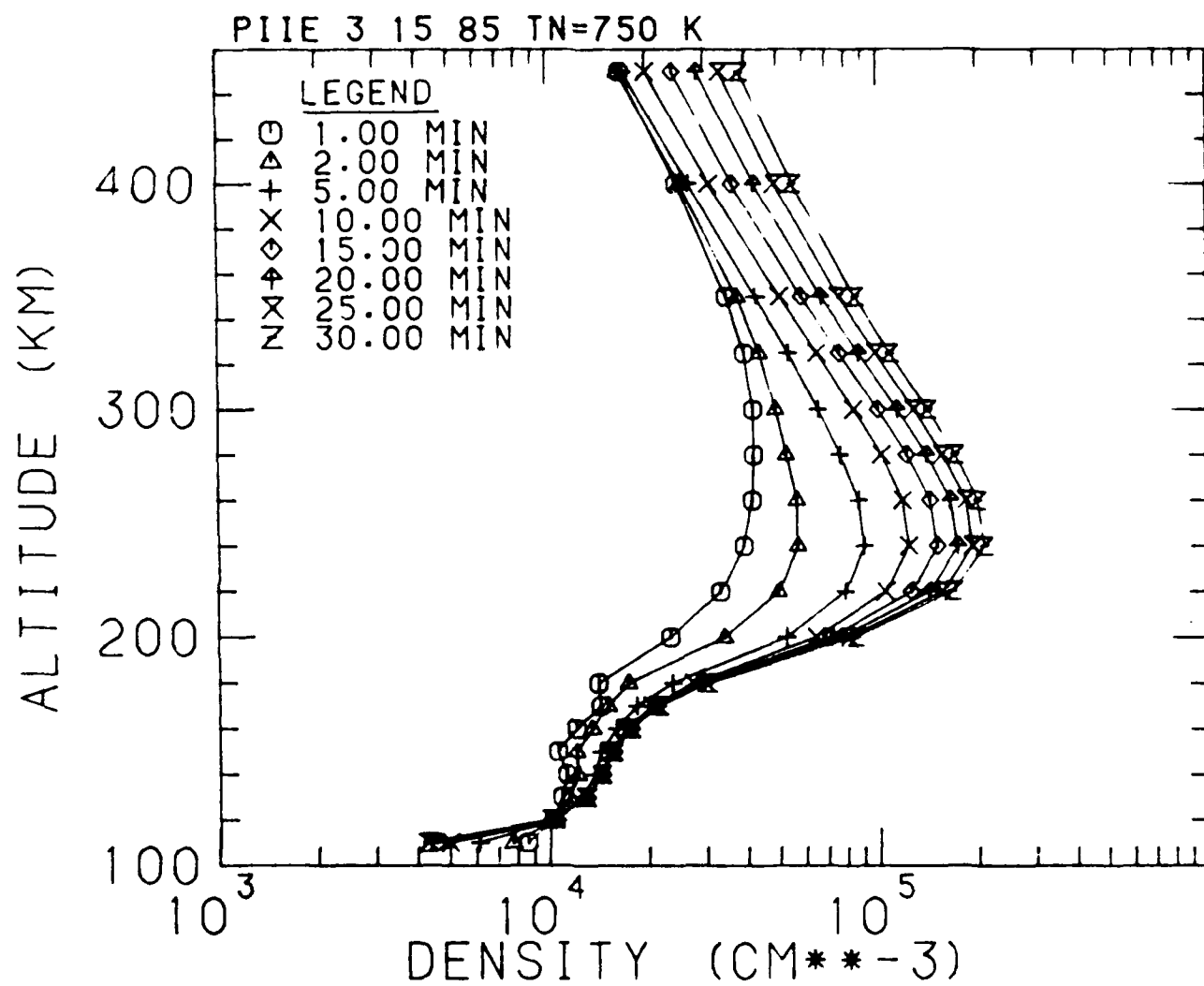


Figure 19

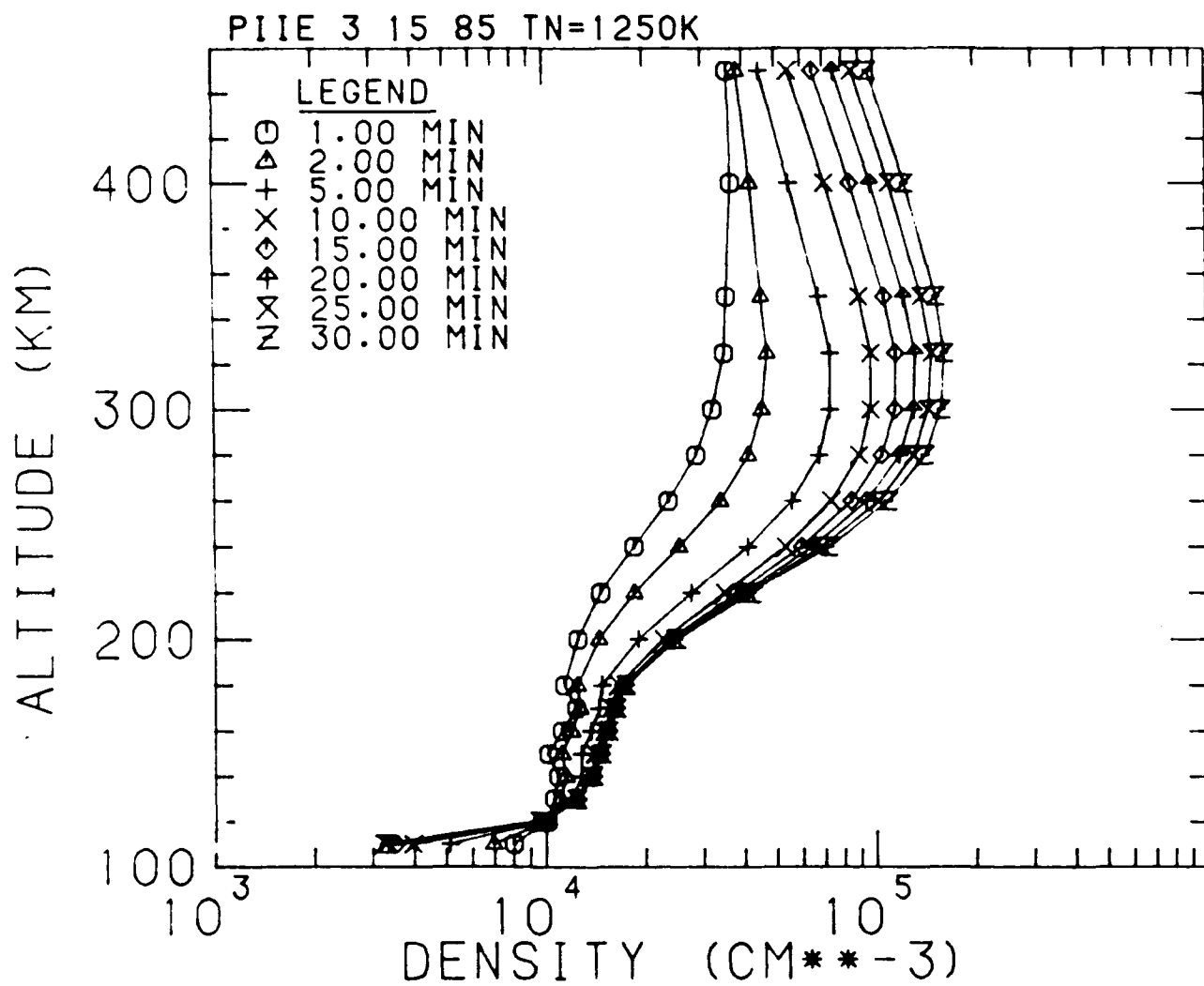


Figure 20